Broad-band X-ray/γ-ray spectra and binary parameters of GX 339−4 and their astrophysical implications

Andrzej A. Zdziarski,[1]* Juri Poutanen,[2] Joanna Mikołajewska,[1] Marek Gierliński,[1,3] Ken Ebisawa[4] and W. Neil Johnson[5]

[1]*N. Copernicus Astronomical Center, Bartycka 18, 00-716 Warsaw, Poland*
[2]*Stockholm Observatory, S-133 36 Saltsjöbaden, Sweden*
[3]*Astronomical Observatory, Jagiellonian University, Orla 171, 30-244 Cracow, Poland*
[4]*Laboratory for High Energy Astrophysics, NASA/Goddard Space Flight Center, Greenbelt, MD 20771, USA*
[5]*E. O. Hulburt Center for Space Research, Naval Research Laboratory, Washington, DC 20375, USA*

ABSTRACT

We present X-ray/γ-ray spectra of the binary GX 339−4 observed in the hard state simultaneously by *Ginga* and *CGRO* OSSE during an outburst in 1991 September. The *Ginga* X-ray spectra are well represented by a power law with a photon spectral index of $\Gamma \simeq 1.75$ and a Compton reflection component with a fluorescent Fe Kα line corresponding to a solid angle of an optically thick, ionized medium of $\sim 0.4 \times 2\pi$. The OSSE data ($\gtrsim 50$ keV) require a sharp high-energy cut-off in the power-law spectrum. The broad-band spectra are very well modelled by repeated Compton scattering in a thermal plasma with an optical depth of $\tau \sim 1$ and $kT \simeq 50$ keV. We also study the distance to the system and find it to be $\gtrsim 3$ kpc, ruling out earlier determinations of ~ 1 kpc. Using this limit, the observed reddening and the orbital period, we find the allowed range of the mass of the primary is consistent with it being a black hole.

We find the data are inconsistent with models of either homogenous or patchy coronae above the surface of an accretion disc. Rather, they are consistent with the presence of an inner hot disc with the viscosity parameter of $\alpha \sim 1$ accreting at a rate close to the maximum set by advection. The hot disc is surrounded by a cold outer disc, which gives rise to the reflection component and a soft X-ray excess, also present in the data. The seed photons for Comptonization are unlikely to be due to thermal synchrotron radiation. Rather, they are supplied by the outer cold disc and/or cold clouds within the hot disc. $e^{\pm}$ pair production is negligible if electrons are thermal. The hot disc model, for which scaled parameters are independent of the black hole mass, is supported by the similarity of the spectrum of GX 339−4 to those of other black hole binaries and Seyfert 1s. On the other hand, their spectra in the soft γ-ray regime are significantly harder than those of weakly magnetized neutron stars. Based on this difference, we propose that the presence of broad-band spectra corresponding to thermal Comptonization with $kT \gtrsim 50$ keV represents a black hole signature.

Key words: accretion, accretion discs – binaries: general – stars: individual: GX 339−4 – gamma-rays: observations – gamma-rays: theory – X-rays: stars.

1 INTRODUCTION

GX 339−4, a bright and well-studied binary X-ray source, is commonly classified as a black hole candidate based on the similarity of its X-ray spectral states and short-time variability to those of Cyg X-1 (e.g. Tanaka & Lewin 1995). However, determinations of the mass of its compact star, M_X, have been inconclusive

(e.g. Cowley, Crampton & Hutchings 1987, hereafter C87; Callanan et al. 1992, hereafter C92), and thus its nature has been uncertain. Therefore, further studies of the properties of GX 339−4, as well as their comparison with those of objects with more direct evidence for harbouring a black hole, is of crucial importance.

In this work, we present two, very similar, broad-band X-ray/γ-ray (hereafter Xγ) spectra of GX 339−4 obtained during a strong outburst of the source in September 1991 (Harmon et al. 1994) simultaneously by *Ginga* (Makino et al. 1987) and the Oriented

*E-mail: aaz@camk.edu.pl

Scintillation Spectroscopy Experiment (OSSE) detector (Johnson et al. 1993) on board the *Compton Gamma Ray Observatory* (*CGRO*). The source was in the hard (also called 'low') spectral state. The *Ginga* and OSSE observations were reported separately by Ueda, Ebisawa & Done (1994, hereafter U94) and Grabelsky et al. (1995, hereafter G95), respectively. However, the data from the two instruments have not been fitted together, and G95 found models with Compton reflection of Xγ photons from an accretion disc unlikely whereas U94 found strong evidence in the *Ginga* data for the presence of this process.

Here, we re-analyse the simultaneous *Ginga* and OSSE data based on the present accurate calibration of those instruments. This leads to a reconciliation of the apparent discrepancies between the data sets from the two instruments, and allows us to fit the joint data with physical models. We also study the distance, reddening, Galactic column density and the masses of the binary members. Those results are then used in studying radiative processes, geometry and physical models of the source. Finally, we find the Xγ spectrum of GX 339−4 similar to those of black hole binaries and Seyfert AGNs, and, in particular, virtually identical to that of NGC 4151, the Seyfert brightest in hard X-rays. This favours physical models with scaled parameters independent of the central mass, such as a hot accretion disc with unsaturated thermal Comptonization (Shapiro, Lightman & Eardley 1976, hereafter S76). On the other hand, the spectrum of GX 339−4 is significantly different from those observed from neutron star binaries, which supports the black hole nature of the compact object in GX 339−4.

2   THE PARAMETERS OF THE BINARY

In order to analyse the X-ray data meaningfully, we need to estimate basic parameters of the binary system. Of importance here are the Galactic column density, N_H, the interstellar reddening, $E(B − V)$, the distance, d (for which published estimates range from 1.3 to 4 kpc), the masses of the primary and secondary, M_X and M_c, respectively, and the inclination (with respect to the normal to the orbital plane), i.

2.1   Reddening and column density

Grindlay (1979) found strong interstellar Na **i** D absorption lines and diffuse interstellar bands at $\lambda \sim$ 5775–5795, 6010, 6176, 6284, and 6376 Å, while C87 found a strong interstellar Ca **ii** K absorption line and diffuse λ4430 Å absorption band. The equivalent widths of these features are consistent with $E(B − V) \simeq$ 1–1.3. From the uncertainties of the published estimates, we derive the weighted mean of

$$E(B − V) = 1.2 \pm 0.1 . \tag{1}$$

The most extended all-sky study of the distribution of neutral H based on high-resolution *IUE* observations of Lyα absorption towards 554 OB stars shows that N_H is well correlated with the column density of dust, measured by $E(B − V)$, with $\langle N_H/E(B − V) \rangle = 4.93 \times 10^{21}$ cm^{-2} mag^{-1} (Diplas & Savage 1994). $E(B − V) = 1.2 \pm 0.1$ derived above thus indicates

$$N_H = (6.0 \pm 0.6) \times 10^{21} \text{cm}^{-2} . \tag{2}$$

This N_H is in excellent agreement with that derived from X-ray data. We obtain $N_H = (6.2 \pm 0.7) \times 10^{21}$ cm^{-2} from the depth of the O edge of $\tau_O = 2.6 \pm 0.3$ measured by Vrtilek et al. (1991), and assuming the O abundance of Anders & Ebihara (1982). On the other hand, Vrtilek et al. (1991) and Ilovaisky et al. (1986) have

obtained $N_H = (6.6 \pm 0.3) \times 10^{21}$ cm^{-2} and $(5.0 \pm 0.7) \times 10^{21}$ cm^{-2} from continuum fits in the soft and hard state, respectively. Those values are less reliable because those authors assumed the continuum models of optically thin thermal bremsstrahlung and a single power law for the corresponding two states. The first model cannot hold for a luminous source based on the standard efficiency argument, and the second model disagrees with *Ginga* data, showing the presence of a strong soft X-ray excess in addition to the harder power law over two orders of magnitude of the flux in the hard state (U94). Therefore, we assume hereafter $N_H = 6 \times 10^{21}$ cm^{-2}, which value agrees with both optical and X-ray data.

On the other hand, Ilovaisky et al. (1986) obtained $E(B − V) = 0.7 \pm 0.1$ by converting their fitted N_H (which appears underestimated, see above) with an old calibration of $N_H/E(B − V)$, which underestimates $E(B − V)(N_H)$ according to the presently most extensive study of Diplas & Savage (1994). This value of $E(B − V)$ is also in disagreement with the results from interstellar features, and it appears incorrect.

2.2   Distance

Obviously, reddening increases with distance. However, the resulting correlation depends sensitively on direction because the distribution of the interstellar matter is very complex and patchy (e.g. Diplas & Savage 1994; Neckel & Klare 1980), especially towards the Galactic Centre, in which direction is the line of sight of GX 339−4.

To illustrate this problem, we show here examples of a wide dispersion of $E(B − V)(d)$ with l, b within $\pm 5°$ from the direction to GX 339−4. That field includes many OB stars in stellar systems, for which both $E(B − V)$ and d have been well studied. First, the distribution of OB stars and dust in a 21-deg^2 field centred at $(l, b) = (335°, 0°)$ was studied in detail by FitzGerald (1987), who found that the dust is distributed in two distinct clouds, one in the local arm at 190 ± 30 pc and the other in an interarm cloud at 690 ± 70 pc with $\langle E(B − V) \rangle = 0.21$ and 0.76, respectively. Three OB associations along this line of sight found at $\langle d \rangle = 1.34$, 2.41 and 3.69 kpc have $E(B − V) = 0.82$, 0.86 and 0.92, respectively. On the other hand, the open clusters NGC 6200, NGC 6204 and Hogg 22 at $(l, b) \simeq (338.5, −1.2)$ show $E(B − V) \lesssim 0.66$ for $d \lesssim 2.78$, while NGC 6193 at $(l, b) = (336.7, −1.6)$ and NGC 6250 at $(340.8, −1.8)$ show $E(B − V) = 0.44$–0.49 at $d = 1.4$ kpc, and $E(B − V) = 0.38$ at $d = 0.95$ kpc, respectively (Moffat & Vogt 1973, 1975; FitzGerald et al. 1977; Vázquez & Feinstein 1992). Finally, the clusters NGC 6208 at $(333.5, −5.7)$, IC 4651 at $(341, −8)$ and NGC 6352 at $(342, −7)$ at $d = 1$, 1.15 and 5 kpc show $E(B − V) = 0.18$, 0.12 and 0.4, respectively (Lindoff 1972; Alcaino 1971). These results clearly show that $E(B − V)(d)$ around GX 339−4 depends sensitively on direction.

Therefore, we have determined $E(B − V)$ and d for ~ 450 stars with $V \lesssim 10$ within $\pm 5°$ around GX 339−4 using their *UBV* magnitudes and spectral types from the catalogue of Mermilliod & Mermilliod (1994). Our study confirms the strong dependence of $E(B − V)(d)$ on direction and allows an accurate determination of $E(B − V)(d, l, b)$ in that field. We have found that $E(B − V)$ depends much more sensitively on b than on l, and thus we present in Fig. 1 our results only for a smaller field centred at GX 339−4 with $(l, b) = (338.9 \pm 5°, −4.3 \pm 1°)$. Stars with $l \lesssim 338°$ and $\gtrsim 340°$ are indicated by open circles and crosses, respectively. Filled circles represent stars in a central field with a radius of $\sim 1°$. From Fig. 1, it is clear that the extinction increases up to $\langle E(B − V) \rangle \approx 0.6$ at $d \approx 2$ kpc. There is a possible further increase beyond ~ 3 kpc, but
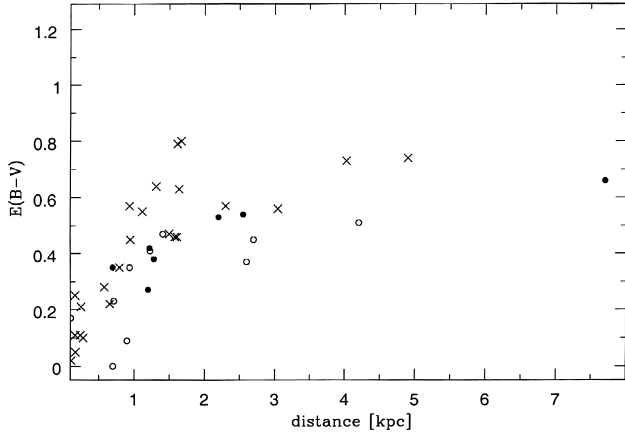
Figure 1. The dependence of $E(B - V)$ on distance in the field centred at GX 339−4. Filled circles represent stars in a small field with a radius of $\sim 1°$ around the source. Two stars closest to the line of sight of GX 339−4 are shown by the two filled circles between 2 and 3 kpc. Crosses and open circles represent nearby sources outside that radius on the side of the Galactic Centre and on the opposite side, respectively. (Note an increase of extinction per unit distance toward the Galactic Centre.) In contrast, the extinction of GX 339−4 is $E(B - V) = 1.2 \pm 0.1$.

to confirm it we would need a deeper survey than that of Mermilliod & Mermilliod (1994). Two stars nearest to GX 339−4 with known *UBV* magnitudes and spectral types are the early B-type giants HD 153222 and CPD −48°11361 at $(l, b) \approx (338°, -4°)$, for which we have found $E(B - V) = 0.53$, $d \gtrsim 2.2$ kpc, and $E(B - V) = 0.54$, $d \simeq 2.6$ kpc, respectively. Thus, our strong conclusion is that GX 339−4 with the measured $E(B - V) = 1.2 \pm 0.1$ must be located at $d > 2.6$ kpc.

This result rules out the most recent estimate of $d = 1.3$ kpc towards GX 339−4, obtained from a *ROSAT* measurement of its X-ray halo by Predehl et al. (1991). They suggest that the halo is produced by a dust cloud near the source, and identify that cloud with the second of two dense clouds found at $d \sim 100–250$ pc and $\sim 800–1400$ pc, respectively, by Neckel & Klare (1980). However, we have not been able to reproduce their identification. There are indeed two clouds shown in the direction of $l = 339°$ in fig. 9 of Neckel & Klare (1980), but that figure gives the cloud distribution *projected* on to the Galactic plane. In fact, table IVa of Neckel & Klare (1980) shows that the field of GX 339−4 (numbered 196 in that paper) does not contribute to extinction in those clouds; also, fig. 8c of that paper shows that A_V at 1 kpc in that field is < 1.9 (whereas $A_V \sim 3.4–4$ corresponds to $E(B - V) = 1.2 \pm 0.1$ of GX 339−4). These findings are confirmed by a more extensive study of Galactic extinction by FitzGerald (1987). She shows that the same clouds are located in the field of Ara OB 1 association at $(l, b) \simeq (335°, 0°)$, confirming that they *do not* concide with the line of sight to GX 339−4. Moreover, the total $E(B - V) \approx 0.8$ at ~ 1.34 kpc (FitzGerald 1987) produced by the two clouds is lower than the $E(B - V) \simeq 1.2$ measured for GX 339−4 (and adopted by Predehl et al. 1991 in their analysis). Similarly, $d = 1.33$ kpc derived by Mauche & Gorenstein (1986) for GX 339−4 from *Einstein* observation of the X-ray halo corresponds just to the dust layer of the Galaxy, and thus it represents a lower limit to the distance. That limit can be actually higher ($d \gtrsim 2$ kpc) since recent studies (Diplas & Savage 1994) show a value of the scaleheight for the dust layer of 150 pc, which is larger than 100 pc adopted by Mauche & Gorenstein. Those two scaleheights predict $E(B - V) \sim 0.5$ and ~ 0.8, respectively, both lower than the $E(B - V)$ of GX 339−4.

On the other hand, the distance to GX 339−4 can be estimated from its systemic velocity of $V_0 = -62 \pm 10$ km s^{-1} (C92). Using the V_0–d conversion chart from Burton (1992), the kinematic distance is $d = 4 \pm 1$ kpc. (Note that a possible peculiar velocity of the system as well as a systematic uncertainty of the above V_0 makes this estimate less secure than the extinction limit.)

We note here that both the studies of distribution of matter in the Galaxy and the measurements of radial velocities of H ii regions in the range $l \approx 300–340°$ indicate the presence of a spiral arm at a distance of ~ 4 kpc (Scheffler & Elsasser 1987 and references therein). Our derived kinematic distance and the relatively large $E(B - V)$ of GX 339−4 are consistent with its location in that arm.

Finally, we can put an upper limit on d from the Eddington limit, which appears to be satisfied in all known black hole binaries (Tanaka & Lewin 1995). The most luminous state of GX 339−4 reported as yet appears to be a soft state in 1988 (Miyamoto et al. 1991), for which we estimate the bolometric flux (using the disc blackbody model, see Section 5.2) to be $\sim 4 \times 10^{-8}$ erg cm^{-2} s^{-1}. This corresponds to $d \simeq 10(L/L_E)^{1/2}(M_X/3M_\odot)^{1/2}$ kpc, where L_E is the Eddington luminosity (see Section 2.3 for discussion of M_X). On the other hand, typical maximum luminosities of black hole binaries are at least a factor of a few below L_E (Tanaka & Lewin 1995), and, e.g. $d \simeq 4.5$ kpc if $L = 0.2L_E$ and $M_X = 3M_\odot$.

Concluding this section, our strongest limit is $d \gtrsim 3$ kpc based on the extinction study. This limit is consistent with the kinematic distance of $d = 4 \pm 1$ kpc and with the Eddington limit. Thus, we adopt $d = 4$ kpc hereafter.

2.3 The masses and geometry

With the above results for $E(B - V)$ and d, we can constrain the mass of the companion star. In general, we expect $M_c \lesssim 1$ M$_\odot$ in low-mass X-ray binaries (hereafter LMXBs, e.g. van Paradijs & McClintock 1995), to which class GX 339−4 most likely belongs. At $d \simeq 4$ kpc and $A_V \sim 3.4–4$, a 1-M$_\odot$ main-sequence star has an observed $V \simeq 20.5–21$ ($B - V \simeq 1.8$, $V - R_c \simeq 1$, $V - I_c \simeq 2$), which corresponds to fluxes below the faintest ones observed as yet from GX 339−4, as illustrated in Fig. 2. Thus, the presence of a $1 - $ M$_\odot$ secondary star is entirely consistent with the present data. We note that our conclusion differs from that of C92, who claimed $M_c \lesssim 0.4$ M$_\odot$. The reason for the discrepancy is that those authors assumed $d = 1.3$ kpc (from Predehl et al. 1991) and $E(B - V) = 0.7$ (from Ilovaisky et al. 1986), of which both values have been found by us to be incorrect, see above.

C92 detected a 14.8-h flux modulation in both optically high and optically low states. They also found the same periodicity in the radial velocities of He ii 4686 and H i Balmer emission lines measured in low-resolution spectra from 1986 May 7–9 (C87). We caution here that interpreting this periodicity as resulting from the orbital period remains relatively uncertain.

First, the periodicity is absent in the radial velocity data from 1985 March 14–17 of C87, although it is possibly due to their poorer quality. Secondly, although C87 claimed that the source was in its 'normal' (high optical) state of ~ 16.5 mag both in 1985 March and 1986 May, C92 noted a displacement in the mean velocity between those data from $\sim + 96$ km s^{-1} to -62 ± 10 km s^{-1}; also, Ilovaisky et al. (1986) reported a relatively faint optical state from late 1985 March ($B \sim 18.8$) through 1985 April 29, which contradicts this claim of C87. Thirdly, Corbet et al. (1987) report strong variability around 1986 May. Namely, their optical photometry from 1986 April and June/July shows variability by several tenths of a magnitude during each observing night and an overall brightening

by 0.5 mag from April to June. On the other hand, the equivalent widths of both He ii 4686 and Hβ lines for both data sets are almost the same (C87), and similar to the mean equivalent widths observed in LMXBs (Smale 1996). However, these lines can be formed in either the heated hemisphere of the secondary, the accretion disc and/or the accretion stream, depending both on the object and/or its state of activity, which precludes an unambiguous interpretation of the spectroscopic periodicity.

Furthermore, we note that C92 do not state whether the 14.8-h periodicity found by them in the (optically) high-state photometry of Corbet et al. (1987) was present in both 1986 April and June/July or in only one of those data sets. C92 also claim that if the maximum in the light curve (presented in their fig. 6) corresponds to transit of the compact object in front of its companion, the radial velocity changes (shown in their fig. 7) are consistent with an origin near the compact object. However, this is not the case because at both spectroscopic conjunctions (i.e. the transits of the compact star both
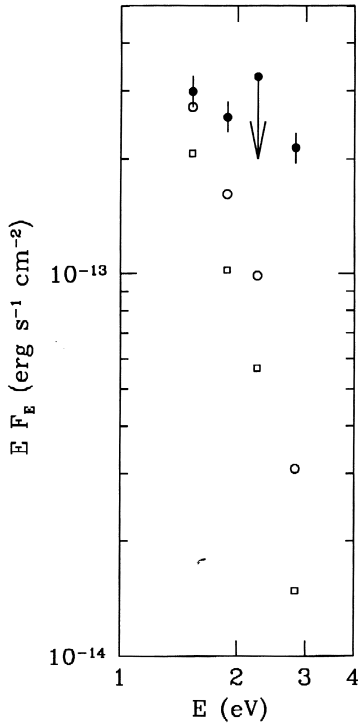

Figure 2. Fluxes at the I_c, R_c, V and B bands (from left to right) of a 1-M$_\odot$ main-sequence star at 4 kpc reddened by $E(B - V) = 1.2$ (open squares) and by $E(B - V) = 1$ (a less likely value; open circles) compared with the faintest observations (not simultaneous) of GX 339−4 (filled circles). The B, V are from Ilovaisky & Chevalier (1981) and Ilovaisky et al. (1986), and R_c, I_c are from C92. For both estimates of $E(B - V)$, the stellar spectrum is below the observations of GX 339−4 (for which the spectrum is a sum of emission from the companion star and from the accretion flow onto the compact object). Thus, the presence of a 1-M$_\odot$ secondary star is fully compatible with the present data.

in front of and behind the companion) the observed radial velocity should be just the systemic velocity.

Keeping these doubts in mind let us tentatively assume that the 14.8-h modulation is still due to the orbital motion. The semi-amplitude, $K_X = 78 \pm 13$ km s^{-1} (C92; the uncertainty is 1σ), implies a secondary mass function of

$$f \equiv \frac{M_c \sin^3 i}{(1 + M_X/M_c)^2} = 0.030^{+0.018}_{-0.012} \text{ M}_\odot, \qquad (3)$$

which corresponds to a mass of the primary of

$$M_X = M_c \left[(M_c/f)^{1/2} \sin^{3/2} i - 1 \right]. \qquad (4)$$

From the lack of eclipses, the inclination can be constrained to $i \lesssim 60°$ (C87). If we adopt $M_c = 1$ M$_\odot$ (see above), we obtain $M_X \lesssim 5$ M$_\odot$, where the equality corresponds to the minimum f and maximum i. On the other hand, the lack of X-ray dips and fits of models with Compton reflection (see Section 4) both favour $< 60°$, and, e.g., $i = 45°$ yields $M_X \lesssim 3.4$ M$_\odot$. Current theoretical (see e.g. Haensel 1995 for a review) and observational (e.g. van Paradijs & McClintock 1995) estimates yield the maximum mass of a neutron star of $\lesssim 2$ M$_\odot$. On the other hand, if we assume that the compact object is a black hole, as strongly suggested by the similarity of its spectral and timing behaviour to Cyg X-1, then the presumed $M_X \gtrsim 2$ M$_\odot$ corresponds to $M_c \gtrsim 0.5$ M$_\odot$ (at the lower limit of f). Thus, the mass function of C92 together with the constraints on M_c is fully consistent with the presence of a black hole in GX 339−4 (although the presence of a neutron star is also allowed). Hereafter, we will adopt fiducial values of $M_X = 3$ M$_\odot$ and $i = 45°$, which are around the middle of the allowed parameter space.

Then, $P_{orb} = 14.8$ h and $M_X + M_c \sim 4$ M$_\odot$ imply a 1.3-R$_\odot$ Roche-lobe (tidal) radius for the secondary. A post-main-sequence 1-M$_\odot$ star with $R \sim 1.3$ R$_\odot$ (and thus filling its Roche lobe) would have a luminosity of ~ 1 L$_\odot$ and an effective temperature (unheated) of ~ 5100 K (Webbink, Rappaport & Savonije 1983). Such a star at $d = 4$ kpc and $E(B - V) = 1.2$ would have $V \sim 21.6$, $B - V \sim 2$, $V - R_c \sim 1.1$, and $V - I_c \sim 2.3$, which corresponds to fluxes lower than those observed from GX 339−4 (similarly to the case of a 1-M$_\odot$ main-sequence star, see Fig. 2). The expected Roche-lobe overflow rate, $\dot{M}$, in such a system is several times 10^{-10} M$_\odot$ yr^{-1} (Webbink et al. 1983), which is sufficient to power the average Xγ emission from GX 339−4 (Rubin et al. 1998) of $\sim 2 \times 10^{36}$ erg s^{-1} assuming an accretion efficiency of $\eta = 0.06$. On the other hand, $\dot{M}$ can be significantly higher due to Xγ irradiation of the companion star (Podsiadlowski 1991; Tavani & London 1993), which would imply a lower η.

In this geometry, the secondary star subtends a solid angle of $\sim 0.018 \times 4\pi$. Thus, the secondary provides a negligible contribution to Compton reflection in GX 339−4 (Section 4).

3 *Ginga* AND OSSE DATA

GX 339−4 was observed by *Ginga* on 1991 September 11 and 12 (U94), and by OSSE on 1991 September 5−12 (G95). We have

Table 1. The log of observations in UT. The counts of *Ginga* and OSSE are for 1.2−29 keV and 50−150 keV energy ranges, respectively. The OSSE exposure and count rate are normalized to one of its four detectors operating during the observations.

Data set	Date	*Ginga* Start	End	Live time [s]	Counts [s^{-1}]	OSSE Start	End	Exposure [s]	Counts [s^{-1}]
1	1991 Sept. 11	03^{h}35^m	05^{h}26^m	1952	1716 ± 4	03^{h}25^m	05^{h}47^m	4795	13.14 ± 0.26
2	1991 Sept. 12	00^{h}54^m	01^{h}11^m	384	1695 ± 5	01^{h}10^m	01^{h}59^m	2488	12.71 ± 0.35

Table 2. The parameters of the fits in Section 4 to the *Ginga* and OSSE data. For each data set, the consecutive fits are to the 4.1–29 keV, 4.1–1000 keV and 1.2–1000 keV ranges, respectively. L and L_{bb} are the unabsorbed bolometric luminosities of the total spectrum and of the blackbody component only, respectively, in units of 10^{37} erg s^{-1}. A is the 1-keV normalization of the primary continuum (in cm^{-2} s^{-1} keV^{-1}), ξ is in erg cm s^{-1}, I_{Fe} is in 10^{-3} cm^{-2} s^{-1}, kT, kT_{bb} are in keV, and W_{Fe} is in eV.

No.	A	Γ	kT	L	$\Omega/2\pi$	ξ	A_{Fe}	kT_{bb}	L_{bb}	E_{Fe}	I_{Fe}	W_{Fe}	χ^2/dof
						1991 September 11							
1a	0.75	$1.75^{+0.02}_{-0.03}$	–	–	$0.37^{+0.06}_{-0.05}$	120^{+160}_{-70}	$2.5^{+1.2}_{-0.8}$	–	–	$6.51^{+0.31}_{-0.32}$	$1.5^{+0.7}_{-0.8}$	49^{+26}_{-26}	11.7/27
1b	0.75	$1.76^{+0.02}_{-0.01}$	56^{+6}_{-6}	–	$0.43^{+0.03}_{-0.07}$	110^{+120}_{-50}	$2.9^{+0.1}_{-0.7}$	–	–	$6.51^{+0.16}_{-0.35}$	$1.3^{+0.8}_{-0.7}$	45^{+26}_{-25}	45.2/79
1c	0.60	$1.77^{+0.01}_{-0.01}$	57^{+7}_{-5}	3.12	$0.44^{+0.06}_{-0.06}$	90^{+90}_{-40}	$3.0^{+0}_{-0.7}$	$0.25^{+0.02}_{-0.03}$	0.29	$6.54^{+0.33}_{-0.36}$	$1.3^{+0.7}_{-0.8}$	44^{+25}_{-26}	47.8/82
						1991 September 12							
2a	0.73	$1.74^{+0.03}_{-0.04}$	–	–	$0.25^{+0.08}_{-0.08}$	230^{+510}_{-180}	$1.6^{+2.2}_{-0.8}$	–	–	$6.56^{+0.34}_{-0.37}$	$1.4^{+0.9}_{-0.9}$	48^{+31}_{-32}	22.4/27
2b	0.75	$1.76^{+0.02}_{-0.02}$	53^{+8}_{-7}	–	$0.29^{+0.09}_{-0.08}$	170^{+310}_{-130}	$2.0^{+1.0}_{-0}$	–	–	$6.57^{+0.37}_{-0.41}$	$1.3^{+0.9}_{-0.9}$	44^{+31}_{-31}	61.5/79
2c	0.55	$1.76^{+0.02}_{-0.03}$	52^{+7}_{-6}	2.93	$0.29^{+0.08}_{-0.08}$	170^{+300}_{-120}	$2.0^{+1.0}_{-0}$	$0.27^{+0.03}_{-0.03}$	0.21	$6.56^{+0.35}_{-0.38}$	$1.4^{+0.8}_{-1.0}$	46^{+30}_{-31}	62.5/82

extracted the OSSE data for September 11 and 12 for periods approximately coinciding with the *Ginga* observations. The log of the *Ginga* (from U94) and OSSE observations used here is given in Table 1. Both the *Ginga* and OSSE fluxes during September 11–12 were approximately constant (U94; G95).

We adopt the current best estimate of the effective area of the Large Area Counter (LAC) of *Ginga* (Turner et al. 1989) of 4661 cm^2 (D. Smith, private communication). The usable energy range of *Ginga* is 1.2–29 keV for these observations. A 1 per cent systematic error is added in quadrature to the statistical error in each *Ginga* channel (as in U94).

The OSSE data are from 50 to 1000 keV. They include energy-dependent systematic errors estimated from the uncertainties in the low-energy calibration and response of the detectors using both in-orbit and pre-launch calibration data, and correspond to an uncertainty in the effective area in the OSSE response. They are most important at the lowest energies (~3 per cent at 50 keV, decreasing to ~0.3 per cent at $\gtrsim$150 keV).

4 ELEMENTARY SPECTRAL MODELS

In this section, we analyse the *Ginga* and OSSE data using idealized models of blackbody emission, and power-law or Comptonization emission from a hot, isotropic, thermal plasma cloud including their Compton reflection from an underlying slab. Here, we assume the reflected component is not Comptonized by the hot plasma. This allows us to characterize spectral components present in the Xγ spectrum in a phenomenological, but relatively model-independent, way. Similar models are widely used in the literature to model spectra of other black hole sources, e.g. Cyg X-1 (Ebisawa et al. 1996) or Seyfert 1s (Nandra & Pounds 1994), and thus the results of this section allow a direct comparison of the obtained parameters with those for other objects. On the other hand, we introduce more realistic geometries in the context of specific models and treat Comptonization of a fraction of the reflected spectrum as well as energy balance in Sections 5.1 and 5.2 below.

For spectral fits, we use **xspec** (Arnaud 1996) v10. The confidence ranges of each model parameter are given for a 90 per cent confidence interval, i.e., $\Delta\chi^2 = 2.7$ (e.g. Press et al. 1992). On the other hand, the plotted vertical error bars are 1σ, the upper limits 2σ, and the plotted spectral data are rebinned for clarity of the display. Model spectra are attenuated by $N_H = 6 \times 10^{21}$ cm^{-2} (Section 2.1). Since the *Ginga* exposure is much longer for the data set 1, we discuss below results obtained with that set. However, we give fit results for both data sets in Table 2.

As found by U94, the *Ginga* spectra of GX 339–4 in the hard state consist of four main components: an underlying power law, a soft excess below ~4 keV, a continuum due to reflection from the surface of an ionized accretion disc (e.g. Lightman & White 1988; George & Fabian 1991), and a fluorescent Fe Kα line.

For modelling Compton reflection, we use the inclination-dependent Green's functions of Magdziarz & Zdziarski (1995) (instead of the angle-averaged reflection spectrum used in U94), which assumes an isotropic point source (or, equivalently, an optically thin corona) above a slab. The Green's functions are convolved with an incident continuum (a power law or a thermal Comptonization spectrum). The reflector inclination is kept at $i = 45°$ (unless stated otherwise). We treat the solid angle, Ω, subtended by the reflector as a free parameter. Values of $\Omega < 2\pi$ may correspond either to a truncation of the reflecting disc, or to substantial Comptonization of the reflected spectrum (or both). The ionization parameter of the reflector, $\xi = L_{ion}/nr^2$, is assumed to be uniform in the reflecting material. Here L_{ion} is defined as the 5 eV–20 keV luminosity in a power-law spectrum and n is the density of the reflector located at distance r from the illuminating source (Done et al. 1992). The reflector temperature is kept at 10^6 K, which is the highest temperature consistent with the model of ionization equilibrium used (Done et al. 1992). This temperature is consistent with our estimate of the origin of reflection from a larger area than that giving rise to the observed soft excess, see Section 5.4. The abundances of both the reflector and the interstellar medium are from Anders & Ebihara (1982) except that the relative Fe abundance in the reflector, A_{Fe}, is a free parameter. The ion edge energies and opacities are from Reilman & Manson (1979, used in U94) except that now the Fe K-edge energies are from Kaastra & Mewe (1993). The continuum reflection is accompanied by an Fe Kα line, which we model as a Gaussian centred at an energy, E_{Fe}, with a width σ_{Fe} and a flux I_{Fe}.

We first fit the data set 1 from *Ginga* in the 4.1–29 keV range only, where a contribution from the soft excess was found to be negligible by U94. We first use a model consisting of a power law and a line. This model provides a very poor description of the data, with $\chi^2 = 209/30$ d.o.f. The pattern of residuals is characteristic of the presence of Compton reflection, as shown in fig. 2a of U94. Indeed, adding a reflection component improves the fit dramatically, reducing χ^2 to 11.7/27 d.o.f.; see fit 1a in Table 2 (which also gives corresponding results for the data set 2) and Fig. 3. Thus Compton reflection is present at very high statistical significance, with a probability of $< 10^{-16}$ that adding this component was not required by the data (as obtained using the F-test). The statistical
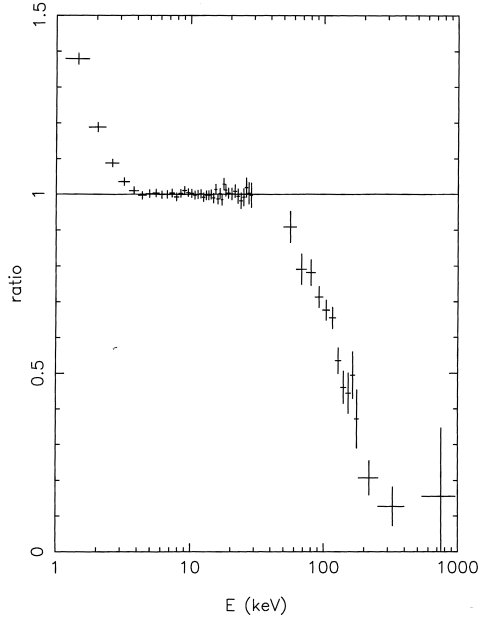
Figure 3. The ratio of the data of 1991 September 11 from *Ginga* and OSSE to the model consisting of a power law, Compton reflection and an Fe Kα line fitted to the *Ginga* data in the 4.1–29 keV energy range.

significances of (i) the reflector being ionized, (ii) the reflector being overabundant in Fe, and (iii) an Fe Kα being present in the spectrum, correspond to the probabilities that the resulting fit improvements were by chance of $< 10^{-4}$, 3×10^{-7} and 3×10^{-4}, respectively. The width of the line is only weakly constrained, $\sigma_{Fe} \lesssim 0.5$ keV at 1σ, and thus we keep it fixed at 0.1 keV hereafter.

We comment here on the low reduced χ^2 obtained for the data set 1. This is due to the 1 per cent systematic error added to the statistical error. This value appears to be an overestimate of the residual inaccuracy of the calibration of the *Ginga* LAC, for which 0.5 per cent appears to be a better estimate. However, we have retained here the statistical error adopted by U94 in order to enable direct comparison with their results. This leads to uncertainties in the parameters of our fits being more conservative than necessary, but it affects neither the best-fitting values nor the conlusions regarding the spectral components present in the *Ginga* spectrum. For example, Compton reflection is still found at a very high significance, see above. The addition of the large systematic error also leads, in some cases, to a relatively low reduced χ^2 for models showing systematic (rather than random) departures from the *Ginga* data, which cases we discuss below individually. On the other hand, the reduced χ^2 is significantly larger for the data set 2, see Table 2. This is due to its much shorter exposure, resulting in typical statistical errors > 1 per cent, which then reduce the relative importance of the systematic errors.

We have then tested whether there is any indication in the data for the presence of kinematic and relativistic smearing of the Fe Kα and the reflection continuum. Such smearing would be present if those spectral components were formed close to the central black hole, which effect has been found in *Ginga* observations of the X-ray novae GS 2023+338 and Nova Muscae (Życki, Done & Smith 1997, 1998). We have used a model in which the line and the static reflection continuum were convolved with the disc line profile of Fabian et al. (1989), similar to the model of Życki et al. (1997, 1978). However, we have found no fit improvement ($\Delta\chi^2 = -0.6$) allowing for the smearing, although the data also do not allow us to rule it out.

The relative normalization of the reflected components, $\Omega/2\pi$, corresponds to ~0.6 of those obtained by U94. This is explained mostly by their use of the angle-averaged spectrum, which underestimates the actual reflection spectrum for angles $< 65°$, which effect increases at energies $\gtrsim 15$ keV (Magdziarz & Zdziarski 1995). Accordingly, the fit to the data set 1 with the angle-averaged reflection in U94 shows strong positive residuals above ~20 keV (fig. 2b in U94); these systematic residuals disappear completely in the present fit, see Fig. 3. Also, we obtain ξ about 2–3 times less than those of U94. However, the ionization state depends on both ξ and the reflector temperature, and the difference is due to the assumption of U94 that the latter is 10^5 K (which seems unlikely in inner regions of luminous compact objects in binaries).

We then investigate the issue of the Fe abundance. We have fitted the earlier four hard-state observations of GX 339−4 by *Ginga* in 1989–90 (U94), and we found all of them consistent with $2 \lesssim A_{Fe} \lesssim 3$, which is also the case for the present data. Therefore, we constrain A_{Fe} to this range hereafter.

In agreement with U94, we find a strong excess below 4 keV, with the fluxes in the 1.2–1.7 keV and 1.7–2.3 keV bands about 40 and 20 per cent, respectively, higher than the extrapolation of the model fitted to the 4.1–29 keV range, as shown in Fig. 3. Although the exact form of the excess depends on the adopted N_H, we find it to be significant, with the respective 1.2–1.7 keV and 1.7–2.3 keV relative excess of 25 and 12 per cent even for $N_H = 4 \times 10^{21}$ cm^{-2}, which is well below the optical and X-ray estimates (Section 2.1). Thus, we conclude that the presence of the soft X-ray excess is not an artefact of our choice of N_H.

At 50 keV, the extrapolated *Ginga* fit predicts a flux about 10 per cent higher than that observed by OSSE. Above 50 keV, the OSSE data show a strong cut-off, as illustrated in Fig. 3. We test whether the cut-off can be modelled by thermal Comptonization, similarly to the case of Cyg X-1 (Gierliński et al. 1997, hereafter G97) and Seyfert AGNs (e.g. Zdziarski et al. 1997, hereafter Z97). We first fit the *Ginga* data above 4.1 keV jointly with the OSSE data. The incident continuum is fitted by thermal Comptonization in a spherical cloud with a central source of soft seed photons having a blackbody distribution, see Zdziarski, Johnson & Magdziarz (1996). As discussed in that paper, the solution of the Kompaneets equation with relativistic corrections used there leads to an overestimation of the actual plasma temperature, T, when the Thomson depth of the plasma, τ, is $\lesssim 2$. Therefore, we correct the values of T obtained from the Kompaneets equation by a function (Misra, Zdziarski & Gierliński, in preparation) obtained by comparison with corresponding Monte Carlo results (Zdziarski et al. 1996). The second parameter of the model is the asymptotic power-law index in X-rays, Γ, which is related to (geometry-dependent) τ by

$$\tau \simeq \Theta^{-1/2}\left[\left(\Gamma + \frac{1}{2}\right)^2 - \frac{9}{4}\right]^{-1/2}, \tag{5}$$

where $\Theta \equiv kT/m_e c^2$ and m_e is the electron mass. In fits, we initially assume the seed photon temperature of $kT_{bb} = 0.1$ keV; as long as kT_{bb} is much less than the minimum energy in the fitted data, its choice does not affect the fit results. This model provides a very good description of the data (see fits 1b and 2b in Table 2). The best fit corresponds to $\tau \simeq 1.8$.

As an independent check of our results, we have also used a model of Coppi (1992), which treats thermal Comptonization using the formalism of escape probability. That model yields $kT \simeq 48$ keV, $\tau \simeq 1.93$, $\Omega/2\pi = 0.42$ as the best fit ($\chi^2 = 49/79$ d.o.f.), rather similar to the fit 1b in Table 2. On the other hand, we find that the high-energy cut-off seen it the data is poorly modelled by an
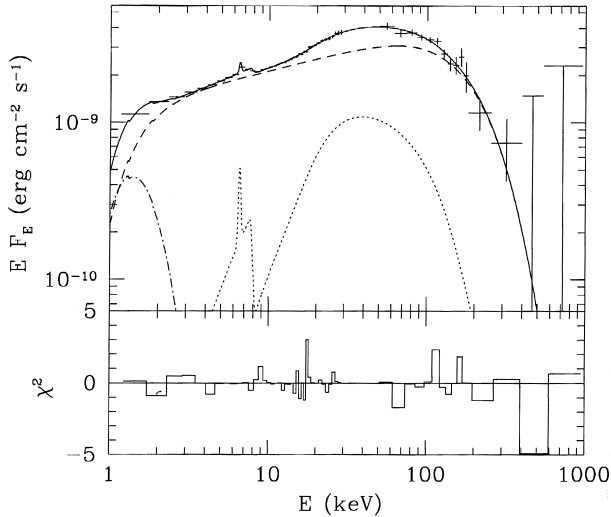
Figure 4. The Xγ spectrum (crosses) of GX 339−4 observed simultaneously by *Ginga* and OSSE on 1991 September 11 (the spectrum of September 12 is very similar and thus it is not shown). The data are fitted by a model consisting of blackbody radiation (dot–dashed curve) providing seeds for thermal Comptonization in a hot plasma (dashed curve). The hard radiation of the hot plasma is Compton-reflected from some cold medium, the component shown by the dotted curve. The solid curve gives the sum. Note that the observed spectrum is attenuated at soft X-rays in the interstellar medium. The bottom panel gives the contribution to the total χ^2 from separate data bins multiplied by the sign of (data − model).

e-folded power law, which, apart from its mathematical simplicity, does not correspond to any physical model. We find that this model fits the data much worse than thermal Comptonization, with $\Delta\chi^2 = +19$ resulting in a systematic pattern of residuals in the OSSE data. This argues for thermal Comptonization indeed being the process giving rise to the intrinsic spectrum.

We have considered the effect of possible inaccuracy of the relative normalization of the effective area of *Ginga* and OSSE. We find, however, no fit improvement, $\Delta\chi^2 = -0.1$, when the relative normalization of OSSE with respect to *Ginga* is allowed to be free (reaching 0.98 for both data sets). Therefore, we keep it at unity hereafter.

We then check the effect of changing the disc inclination. We find that allowing a free i leads to a negligible fit improvement: $\chi^2 = 44.3/78$ d.o.f. at $i = 23^{+38}_{-23}$ degrees. Thus, we keep it at $i = 45°$ (see Section 2.3) hereafter. At the largest i allowed by the fit, $\Omega/2\pi = 0.62$ and $W_{Fe} = 35$ eV.

We then consider the soft X-ray excess. In the hard state of Cyg X-1, the soft excess contains a blackbody component with $kT_{bb} \approx 0.14$ keV (e.g. Ebisawa et al. 1996). In addition, the *ASCA* data for Cyg X-1 show also a break around 3–4 keV with the power law below the break being softer by $\Delta\Gamma \sim 0.4$ on average (Ebisawa et al. 1996). The physical origin of that spectral break is unclear. We find that the soft X-ray excess in our data is much better fitted by an additional blackbody component than by a broken power law ($\Delta\chi^2 = 5$). (Our data extend down to 1.2 keV only with a low energy resolution, and thus do not allow us to determine the presence of more than one spectral component of the soft excess.) In the model with a blackbody component, we set its temperature equal to the blackbody temperature of the seed photons in the Comptonization source. (We postpone examining the energy balance of the source to Sections 5.1 and 5.2 below.) This model gives an excellent description of the *Ginga*/OSSE data in the entire energy range, 1.2–1000 keV; see Fig. 4 and fits 1c and 2c in Table 2. Still,

according to the above discussion, the fitted value of kT_{bb} is relatively uncertain; if there were a low-energy break in the power-law spectral component (as in Cyg X-1), kT_{bb} would be lower.

5 PHYSICAL IMPLICATIONS

5.1 Geometry and energy balance

We now consider thermal Comptonization, Compton reflection and reprocessing in realistic geometries approximating the structure of an accretion flow. We take into account anisotropy of both seed and Compton-scattered photons, Comptonization of the reflected photons that return to the hot plasma, and energy balance.

In general, thermal Comptonization takes place in a hot plasma cloud, and the resulting spectrum is Compton-reflected from a cold medium. A major part of the Comptonized flux incident on the cold medium is bound–free absorbed rather than reflected, which gives rise to a flux of reprocessed soft photons with a spectrum close to a blackbody. In turn, a geometry-dependent fraction of the reflected and blackbody emission returns to the hot plasma. These blackbody photons then serve as seeds for thermal Compton upscattering (in addition to any other soft photons present). Those reflected photons that return to the hot plasma are upscattered, which leads to a strong suppression of that component for $\tau \gtrsim 1$.

A geometry can be ruled out either if the resulting model spectrum does not provide a good fit to the observed spectrum, or if energy balance between the hot plasma and the source of seed photons cannot be achieved. The condition of energy balance can be expressed as, e.g., the power in soft photons incident on the hot plasma (hereafter seed photons) times the Comptonization amplification factor (a function of kT and τ), which is equal to the power emitted by the hot plasma, L_{hot}. The flux in seed photons arises due to both internal dissipation and reprocessing of the Comptonized radiation. Then, a sufficient condition to reject a model is (i) the Comptonized flux (at fitted kT and τ) is larger than that observed, due to a strong flux in seed photons arising from reprocessing. The condition (i) is equivalent to either statement (ii) at the fitted τ and the observed hard flux, Compton cooling by the seed photons would result in a kT less than that obtained from fitting, or (iii) at the fitted kT and the observed hard flux, energy balance can be achieved for values of τ less than that fitted to the data (e.g. Haardt & Maraschi 1993; Stern et al. 1995). Below, we first obtain kT and τ by spectral fitting, and then a posteriori check the energy balance by finding the equilibrium temperature corresponding to the fitted τ in the given geometry [condition (ii) above].

In this section, we neglect spectral constraints from the soft X-ray excess (but return to this issue in Section 5.2 below) because the origin of the observed soft excess is relatively uncertain, see the end of Section 4. Therefore, we consider now only the data above 4 keV, and fix the seed-photon temperature at $kT_{bb} = 0.25$ keV (as obtained in Table 2), which is about the highest seed-photon temperature allowed by the data regardless of the actual form of the soft excess. For a lower kT_{bb} at a given seed-photon flux from reprocessing, the predicted Comptonized flux would increase, which would in turn lead to rejection of a larger class of models [see condition (i) above]. Thus, setting $kT_{bb} = 0.25$ keV is the most conservative assumption for model rejection.

To model Comptonization in anisotropic geometries, we use the iterative scattering method of Poutanen & Svensson (1996). For Compton reflection, we use the same method as in Section 4 (Magdziarz & Zdziarski 1995). Fig. 5 shows the geometries considered in Sections 5.1–5.2.
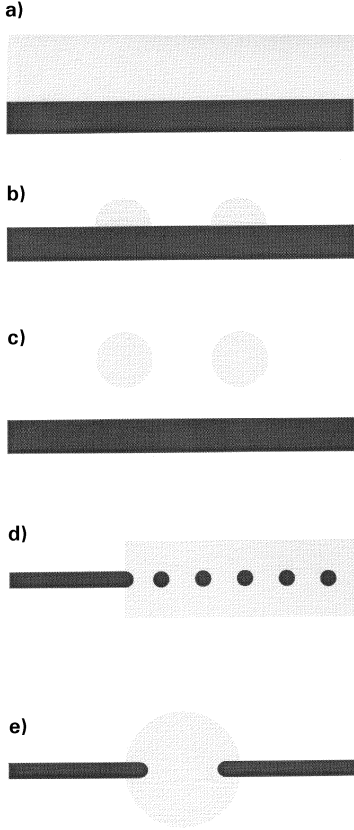
Figure 5. Geometries of the Xγ source considered in Sections 5.1 and 5.2. Dark and light shades denote cold medium and hot plasma, respectively. (a) A homogeneous corona above a disc, (b) active regions located on the disc, (c) active regions detached from the disc, (d) cold clouds in the mid-plane of a hot disc, and (e) a hot central sphere surrounded by a cold disc, which may penetrate some distance within the sphere.

We first consider a homogeneous corona (with the vertical optical depth of τ) covering a cold slab (Haardt & Maraschi 1993), see Fig. 5(a). In this model, all Compton-reflected radiation emitted by the cold slab is Comptonized in the hot corona, which leads to a suppression of this component to a level much less than that present in the data. Still, the model can provide a good spectral fit if we allow an additional Compton reflection component (with $\Omega/2\pi \sim 0.3$) due to an outside cold medium, e.g. an outer cold disc. The fitted plasma parameters are then $kT = 55^{+8}_{-7}$ keV and $\tau = 1.2^{+0.2}_{-0.3}$ ($\chi^2 = 45/79$ d.o.f.). However, this model is strongly ruled out by the requirement of energy balance. Namely, the reprocessed flux from the slab is so strong that it would cool down the corona to ~ 27 keV. Allowing for internal dissipation in the cold slab (presumably a cold accretion disc) would worsen the discrepancy.

We then consider a patchy corona geometry (Galeev, Rosner & Vaiana 1979; Haardt, Maraschi & Ghisellini 1994; Stern et al. 1995). The hot plasma is postulated here to form active regions above a cold accretion disc. First, we assume the active regions to form hemispheres located directly on the surface of the cold disc, see Fig. 5(b). We obtain a good spectral fit ($\chi^2 = 47/79$ d.o.f.) for $kT = 64^{+9}_{-8}$ keV and the radial $\tau = 2.1^{+0.2}_{-0.3}$. However, similarly to the case of a homogeneous corona, we find that cooling by the seed photons arising from reprocessing in an underlying part of disc is so large that the plasma with the fitted τ would cool to $kT = 45$ keV, i.e. it cannot sustain the temperature implied by the data in this model.

The cooling, however, can be reduced if the active regions are at some distance above the disc, as shown in Fig. 5(c). We find that at the height of about one radius, there is an energy balance between the disc without internal dissipation and the hot region. The height has to be larger if there is internal dissipation in the disc. However, this model implies much more Compton reflection (from disc regions surrounding the active region) than observed. Even if we assume that the underlying disc is truncated, which would reduce the amount of reflection, the spectral fit of this model is much poorer than other models, $\chi^2 = 53/79$ d.o.f. (for $kT = 62^{+14}_{-4}$ keV, $\tau = 2.2^{+0.2}_{-0.3}$, $\Omega/2\pi = 0.71^{+0.10}_{-0.07}$). The cause of the bad fit is the presence of an anisotropy break in the model spectrum, i.e. a deficiency of low-energy photons emitted upward due to an anisotropic suppression of the first order of Compton scattering (Haardt & Maraschi 1993; Poutanen & Svensson 1996). This effect is not seen in the data, and thus this model yields systematic departures from the *Ginga* data at low energies. On the other hand, a good fit can be obtained if $kT_{bb} \lesssim 0.1$ keV is assumed (which yields $kT = 57^{+6}_{-4}$ keV, $\tau = 2.5^{+0.3}_{-0.2}$, $\Omega/2\pi = 0.67^{+0.07}_{-0.09}$, $\chi^2 = 45/79$ d.o.f.), in which case the effect of the anisotropy break on the model spectrum does not extend above 4 keV. The weak Compton reflection required by the model could then correspond to the cold disc being truncated around the active region, and the origin of the soft X-ray excess has to be due to an effect different from the disc blackbody emission. Thus, in this respect, the model is in principle possible.

However, U94 found that Ω in GX 339−4 correlates positively with Γ, a behaviour opposite to that expected in the patchy corona model. We first note that since $\tau \gtrsim 2$ in this model, virtually all Compton-reflected photons passing through an active region are removed from the observed reflected spectrum regardless of the exact value of τ. On the other hand, a decrease of the observed Ω can occur when the height of the active region decreases, due to fewer reflected photons being able to escape without hitting the hot plasma. This also will soften the spectrum due to the increased cooling by the larger number of blackbody photons emitted by the disc intercepted by the hot plasma. The observed opposite correlation provides then strong evidence against the patchy corona model.

On the other hand, the data can be well modelled in all respects by a geometry with cold clouds inside a hot slab (S76; Celotti, Fabian & Rees 1992; Kuncic, Celotti & Rees 1997; Collin-Souffrin et al. 1996; Krolik 1998) surrounded by a cold disc, see Fig. 5(d). We assume that the clouds are located in the slab mid-plane and cover a fraction of f_c of the mid-plane. If there is neither dissipation in the cold clouds nor outside seed photons, a solution satisfying both the energy balance and spectral constraints corresponds to $f_c \simeq 0.3$, see Fig. 6. The plasma parameters are then $kT = 51^{+7}_{-3}$ keV and $\tau = 0.95^{+0.13}_{-0.15}$, corresponding to the half-thickness of the slab (at $\chi^2 = 45/79$ d.o.f.). Compton reflection by the cold clouds is attenuated by the hot plasma and thus we need the presence of additional Compton reflection from outside matter with $\Omega/2\pi \simeq 0.4$ (see Table 2). This can occur due to reflection of the radiation of the hot flow by an outside cold disc. The covering factor by the cold clouds will be $f_c < 0.3$ if additional soft photons from the outside cold disc and/or from dissipation in the cold clouds (with the luminosity $L_{bb,intr}$) enter the hot flow, see Fig. 6.

As argued by S76, the clouds can be formed by the radiation-pressure-induced instability of an optically thick disc (Lightman & Eardley 1974; Shakura & Sunyaev 976). The clouds are in pressure equilibrium with the hot medium.

We have also tested a similar geometry with the hot plasma forming a central hot sphere (rather than a slab) surrounded by a
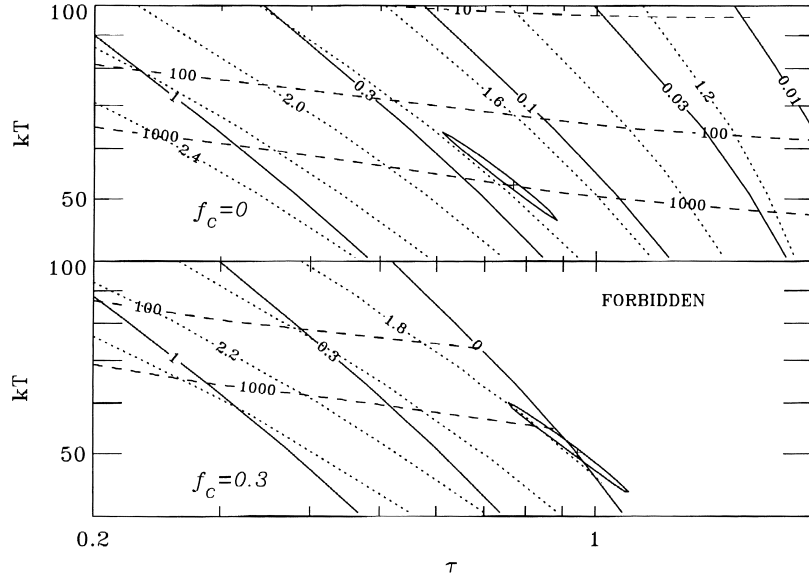
Figure 6. Relations between the electron temperature, kT, and the half-thickness optical depth, τ, of a hot slab; see Fig. 5(d) and Section 5.1. The covering factor of cold clouds in the mid-plane of the hot slab is $f_c \rightarrow 0$ (upper panel) and $f_c = 0.3$ (lower panel). The solid curves correspond to constant $L_{bb,intr}/L_{hot}$, i.e. the ratio of the internally generated and/or external soft luminosity to the dissipation rate in the hot disc. These relations do not depend on the number of $e^{\pm}$ pairs. The dashed curves correspond to a constant local hard compactness, ℓ (assuming pair-dominated thermal plasma, see Section 5.6). The dotted curves correspond to a constant intrinsic (i.e. without Compton reflection) spectral index Γ in the 4–20 keV range. Crosses are the best fits to the data and elongated confidence contours are for 90 per cent confidence for two parameters ($\Delta\chi^2 = 4.61$). For $f_c \rightarrow 0$, the seed-photon luminosity entering the hot slab is ~0.23 of the heating rate, L_{hot}. The covering factor of $f_c = 0.3$ is the largest energetically possible consistent with the data. In that case, no internal dissipation in the cold clouds and no external soft photons are allowed, and cooling is provided by reprocessed radiation only.

cold disc (e.g. Poutanen, Krolik & Ryde 1997), see Fig. 5(e). If the cold disc does not penetrate into the hot cloud, $kT = 57^{+6}_{-3}$ keV and the radial $\tau = 2.0^{+0.1}_{-0.2}$ ($\chi^2 = 47/79$ d.o.f.), and internal dissipation in the cold disc is required to provide enough seed soft photons. The model also predicts less Compton reflection than observed, which problem may be solved by flaring of the outside disc. The cold-disc solution of Shakura & Sunyaev (1973) does, in fact, correspond to a flared disc, and the illumination by the central hot source will further increase the amount of flaring. We note that a central hot sphere is a poor approximation to the actual geometry of a hot accretion flow with substantial cooling (see Section 5.3), in which the scaleheight is maximized at the outer boundary rather than at the centre, which effect will also lead to an increase of the amount of reflected X-rays. We also find that models with the cold disc penetrating into the hot cloud down to $\gtrsim 0.7$ of the sphere radius can also fit the data and satisfy the energy balance, but with less or no dissipation in the cold disc. An overlap between the cold and hot phases increases the amount of Compton reflection in the model and thus reduces the $\Omega/2\pi$ needed from flaring of the outside cold disc.

The Ω versus Γ correlation found by U94 may be explained naturally by the geometries shown in Figs 5(d) and (e). In these geometries, an increase of the area of the outside soft X-ray emitter leads to an increase of the seed-photon flux incident on the hot plasma, which in turn leads to more cooling and softening of the X-ray spectrum, i.e. an increase of Γ. The same effect leads to more Compton reflection, i.e. an increase of Ω.

Summarizing this section, our best models consist of a central hot region surrounded by a cold disc (Figs 5d and e). These models require the presence of an additional Compton reflection component, e.g. from an outer cold disc. Of these two models, a hot disc with cold clouds inside surrounded by a cold disc (Fig. 5d) is more likely to be formed by an accretion flow with substantial cooling (see Section 5.3 below). Both models explain the Ω–Γ correlation.

On the other hand, a model consisting of active regions at some height above a cold disc (Fig. 5c) is marginally possible, but it requires the temperature of blackbody photons to be lower than that inferred from the soft X-ray excess and a truncation of the underlying disc, and it predicts an Ω–Γ correlation opposite to that observed. Models with a homogeneous corona and with the active regions on the disc surface (Figs 5a and b) are strongly ruled out by the requirement of energy balance.

5.2   The origin of the soft X-ray excess

In this section, we fit the data in the full 1.2–1000 keV range, i.e. including the range < 4 keV showing the soft X-ray excess. Based on the results of Section 5.1, the most likely geometry of the hot plasma is a hot inner disc mixed with cold clouds. We first check whether the soft excess can be accounted for just by the emission of the cold clouds, which we find energetically viable. However, this model fits the data much worse than our baseline model of Table 2, $\Delta\chi^2 = +9$, even for the maximum possible covering factor of the cold clouds (see Fig. 6), $f_c = 0.3$.

On the other hand, the hot disc is surrounded by a cold outer disc beyond a transition radius R_{tr} (Fig. 5d), which contributes to the soft excess. We have thus added to our spectral model an integral of blackbody spectra over the disc surface at $R \gtrsim R_{tr}$. The local colour temperature is in general larger than the effective one, and the ratio of the two for best estimates of the system parameters (Section 2) is $T_{colour}/T_{eff} \simeq 1.8$ (Shimura & Takahara 1995). Following Makishima et al. (1986), we neglect here the boundary-condition factor $J(r) \equiv 1 - (6/r)^{1/2}$, where $r \equiv Rc^2/GM_X$, which is a good approximation for a large enough r_{tr}. We find that due to the limited energy range of the *Ginga* data, our fits cannot determine the value of R_{tr}. On the other hand, R_{tr} can be obtained from the area covered by the cold-cloud-emitting blackbody spectrum with the fitted

Table 3. The main parameters of our best model, consisting of a hot inner disc with internal cold clouds surrounded by a cold disc, fitted to the data set 1. See Figs 5(d), 7 and Section 5.2. Temperatures are in units of keV.

τ	kT	f_c	kT_{bb}	kT_{tr}	χ^2/dof
$0.88^{+0.10}_{-0.10}$	52^{+1}_{-3}	$0.26^{+0.04}_{-0.11}$	$0.33^{+0.02}_{-0.04}$	$0.21^{+0.01}_{-0.01}$	$48.6/81$
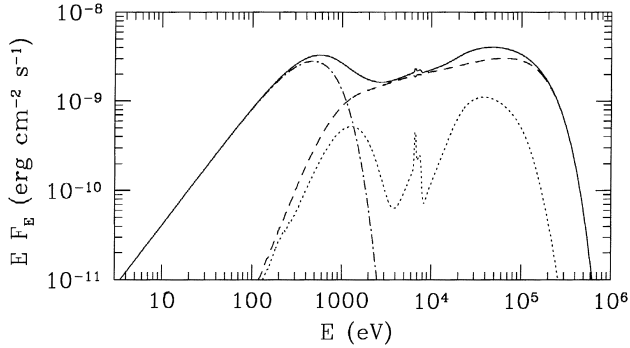
Figure 7. The unabsorbed model spectrum corresponding to the fit to the data of our best model, a hot disc surrounded by a cold disc, see Fig. 5(d). The dot–dashed curve corresponds to the disc–blackbody emission, the dashed curve gives the Comptonized emission in the hot disc, and the dotted curve gives the sum of the blackbody emission of the cold clouds within the hot disc and the reflected component from both the clouds and the cold disc. The solid curve gives the total spectrum.

colour temperature, kT_{bb}. This yields $R_{tr} \simeq 6 \times 10^7$ cm as the best fit. The main model parameters are given in Table 3, where kT_{tr} is the cold disc temperature at R_{tr}, and Compton reflection is from the cold disc. The model spectrum is shown in Fig. 7. The bolometric luminosity is 4×10^{37} erg s^{-1}, and the ratio of the blackbody luminosity of the cold disc to the total one (but without including the outside reflection component) is $\simeq 0.30$.

We point out that we have neglected the effect of heating by the central source on the radial temperature dependence of the outside cold disc. This may significantly soften the power-law part of the disc–blackbody spectrum shown in Fig. 7 (e.g. Vrtilek et al. 1990).

A model alternative to the hot inner disc that was found by us to be marginally possible (Section 5.1) is active regions at some height above the disc (Fig. 5c). In this model, the soft excess can be accounted for by the blackbody emission of the disc region underneath the active region. Due to the intensive heating by the X-rays, the local temperature can be well above the temperature of a disc with internal dissipation only. From the strength of the blackbody component (Table 2), the characteristic size of the heated region of the disc is $\sim 10^7 (T_{colour}/T_{eff})^2$ cm. However, when we approximate the emission of the underlying region of the disc as a blackbody, a very poor fit to the data is obtained, $\chi^2 = 93/82$ d.o.f. This provides one more argument against this model.

Summarizing this section, the most likely origin of the soft excess we have found is from an outer cold accretion disc with an additional contribution from cold clouds within the hot disc, see Figs 5(d) and 7.

5.3 Accretion disc solutions

The best overall model found in Sections 5.1 and 5.2 consists of a hot plasma slab with half-thickness corresponding to $\tau \lesssim 1$, and $kT \gtrsim 50$ keV. Physically, this geometrical model likely corresponds to a hot accretion disc. We note that indeed the best-fitting parameters of the hot slab are close to those predicted by the
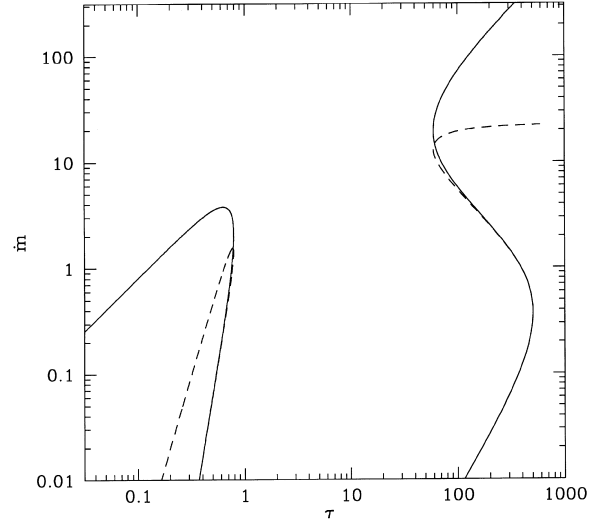

Figure 8. Accretion disc solutions at $r = 13$. The optically thin solution (Z98) is given for $y = 0.33$ and $\alpha = 1$. We identify the observed state of GX 339–4 with the maximum of this solution. For comparison, we also show the optically thick solution (Shakura & Sunyaev 1973; Abramowicz et al. 1988) computed for the same α and $M = 3$ M$_\odot$. Solid curves give the accreted $\dot{m}$ whereas the dashed curves give the part of $\dot{m}$ which is locally converted into escaping radiation. The remaining part of the locally dissipated energy is advected into the black hole.

two-temperature, hot disc model of S76. In that model, the local gravitational energy is converted into the thermal energy of ions (at a temperature $T_i \gg T$), which is then transferred to electrons by Coulomb interactions. The electrons, in turn, radiate away their energy by Compton-upscattering seed photons irradiating the plasma. As found by e.g. Ichimaru (1977), Abramowicz et al. (1995) and Narayan & Yi (1995), advection of hot ions to the black hole leads to another branch of the hot solution as well as limiting the accretion rate possible in the hot flow.

Detailed properties of the solution in the vicinity of the maximum accretion rate are studied by Zdziarski (1998, hereafter Z98). That study follows S76 in characterizing the flow by a value of the Compton parameter, $y \equiv 4\Theta \max(\tau, \tau^2)$ (e.g. Rybicki & Lightman 1979), which approximately determines the X-ray spectral index, Γ. This is equivalent to assuming that the flux in the seed photons is such that it gives rise to an X-ray spectrum with that Γ.

Other parameters of the flow are $\dot{M}$ and the viscosity parameter, α (Shakura & Sunyaev 1973). [The rate of advection is characterized by a parameter $\xi_{adv} \simeq 1$, e.g. Chen, Abramowicz & Lasota (1997).] Z98 has obtained that the optical depth (corresponding to the scaleheight, H) of the flow weakly depends on R, and that τ at the local maximum rate, $\dot{M}_{max}$, and the maximum τ (see Fig. 8) are

$$\tau(\dot{M}_{max}) \simeq 1.22 y^{3/5} \alpha^{2/5}, \qquad \tau_{max} \simeq 1.54 y^{3/5} \alpha^{2/5}, \qquad (6)$$

respectively. Those values are reached at $r \simeq 13$, at which value the rate of dissipation per logarithmic radius interval is also close to maximum. At $\dot{M}_{max}$, advection carries about half the dissipated power and $H/R \sim 1$.

The luminosity of GX 339–4 during the observations reported is about the maximum observed in the hard state (Harmon et al. 1994; Rubin et al. 1998). Thus, we can relate the above τ to that obtained from fitting the slab model in Section 5.1. We assume here an intermediate value of the covering factor, $f_c = 0.1$ (see Fig. 6), for which $kT = 52^{+7}_{-5}$ keV, $\tau = 0.82^{+0.10}_{-0.12}$ ($\chi^2 = 45/79$ d.o.f.), implying $y = 0.33$. Equating the fitted τ to τ_{max}, we obtain $\alpha \simeq 1$, which is

relatively large [as appears generally to be the case in luminous black hole systems (Narayan 1996)]. Fig. 8 shows the relation between τ and $\dot{m}$ ($\equiv \dot{M}c^2/L_E$) for those y and α; we see that $\dot{m}_{max} \simeq 4$.

The maximum possible luminosity from the hot flow corresponds to the local accretion rate at the maximum set by advection (Fig. 8), for which radial integration implies

$$L_{hot} \lesssim 0.15 y^{3/5} \alpha^{7/5} L_E \tag{7}$$

(Z98). For the luminosity in Table 2, this relation yields $M_X \gtrsim 2.5\,M_\odot$, which is compatible with our estimates of the black hole mass in Section 2. For example, $L_{hot} \simeq 0.06 L_E$ at $M_X = 3\,M_\odot$.

Based on our data for GX 339−4 alone, we cannot distinguish which branch of the optically thin solution (Fig. 8) the source follows in the hard state at luminosities lower than the maximum. In the α model, the advective branch is stable (e.g. Wu 1997) whereas the cooling-dominated branch is unstable (Pringle 1976), but the validity of those predictions has not been tested observationally yet. We point out that if the flux variability in the hard state within a factor of ∼50 (see U94) corresponds to the advective branch of the disc solution, the average accretion rate in the hot flow is within a factor of ∼2 of $\dot{M}_{max}$ (compare the left-hand dashed and solid curves in Fig. 8). The corresponding large $\langle \dot{M} \rangle$ then requires the presence of a radiation-driven outflow from the companion star for our derived system parameters, see Section 2.3.

The formation of the hot disc might be related to the instability of the cold disc in the inner part dominated by radiation pressure (Lightman & Eardley 1974; Shakura & Sunyaev 1976). If this is the case, the transition radius is given by

$$\frac{r_{tr}}{J(r_{tr})^{16/21}} \approx 60(\alpha M_X/M_\odot)^{2/21} \dot{m}^{16/21} \tag{8}$$

(e.g. Svensson & Zdziarski 1994), where α is the viscosity parameter in the cold disc, not necessarily the same as that in the hot one. For $\dot{m} \simeq 4$ and $\alpha \simeq 1$, $r_{tr} \sim 200$.

Our best-fitting model has $L_{bb}/L \simeq 0.3$, see Section 5.2. If the flow is on average ∼50 per cent advective, $L_{bb}/L \sim 50/r_{tr}$ ($r_{tr} \gg 50$), which then implies $r_{tr} \sim 150$, in good agreement with equation (8) above. Then $R_{tr} = 6 \times 10^7$ cm obtained in Section 5.2 corresponds to $M_X \sim 3$, in good agreement with other estimates of M_X here.

5.4 The physical state of the reflecting medium

The region of formation of the Fe Kα line is strongly ionized (Section 4, see also U94). From the best-fitting ionization parameters obtained in Table 2, we find that the dominant Fe ions are Fe **xix** and Fe **xx** for the first and second observation, respectively. Those ions cannot, however, produce the observed line because of the very strong resonant absorption (Matt, Fabian & Ross 1993; Życki & Czerny 1994). The observed line is produced by the non-resonant Fe ions $\leq$ **xvi**. We have computed that those ions constitute about 20 per cent of all iron in the reflecting medium, which explains the weakness of the line. The observed line equivalent width of ∼40 eV is then fully consistent with theoretical calculations for $A_{Fe} \sim 3$, $\Omega/2\pi \simeq 0.4$ and the obtained ionization state of the medium; see Życki & Czerny (1994), George & Fabian (1991) and Matt et al. (1993). The fact that we did not require redshifts of the line centre energy or intrinsic line broadening is consistent with the line origin being at large distances from the black hole, $r \gg 1$.

We can also obtain an estimate of the transition radius from the ionization state of the reflector. The density, n, corresponding to unit Thomson optical depth (where most of the Compton reflection takes place) can be calculated from the vertical structure of the standard cold disc (Milson, Chen & Taam 1994). For example, for $M_X = 3\,M_\odot$ and $\dot{m} = 3$, $n = 1.8 \times 10^{20}$ cm^{-3}, 6.0×10^{19} cm^{-3}, 1.8×10^{19} cm^{-3} and 1.9×10^{17} cm^{-3} at $r = 20$, 60, 200 and 2000, respectively. If there is a central hot disc irradiating the outer cold disc, we can estimate the distance between the illuminating source and the disc region where most of reflection takes place to be roughly equal to the transition radius. The illuminating luminosity on each side of the disc is ∼$(1/2)(\Omega/2\pi)L_{hot}$. From that we obtain $\xi \simeq 1200$, 500, 120 and 120 erg cm s^{-1} at the four values of r above, respectively. Thus, we see that $r_{tr} \gtrsim 10^2$ is compatible with the fitted values of ξ (see Table 2).

On the other hand, the illuminating luminosity is just L_{hot} in the model of an active region above the disc (Fig. 5c). From energy balance, we found that such an active region is located at the height corresponding to its size (Section 5.1), and this height has to be < R. Then, using the values of density from above, we find $\xi \gtrsim 2000$ erg cm s^{-1} at $r \lesssim 100$. Thus, the disc ionization expected in the active region model is much more than that observed. If there are $k > 1$ active regions with a typical luminosity of L_{hot}/k, the typical size (and thus, the height) of the active region must be at least $< R/k^{1/2}$ to fit on the disc surface, and thus the above estimate of ξ remains unchanged. This estimate provides one more argument against the active region model. We caution, however, that the above results have been obtained using our highly simplified model of photo-ionization (see Done et al. 1992).

Our conclusions here differ from those of U94, who estimated that reflection originates in a region at $r \sim 10$. The difference arises because U94 used the average disc density (which is $\gg$ the photo-sphere density) as well as underestimating $\dot{m}$ by using the luminosity in the *Ginga* energy range only and neglecting advection.

5.5 The role of magnetic fields

So far, we have neglected in our treatment any magnetic fields that may be present in GX 339−4 (Fabian et al. 1982; Di Matteo, Celotti & Fabian 1997). If present, thermal synchrotron radiation will provide additional seed photons for thermal Comptonization (Zdziarski 1985, 1986), and this process has been suggested to play a major role in luminous black hole sources (e.g. Narayan 1996; Di Matteo et al. 1997). For kT and τ typical of compact objects, the synchrotron radiation is self-absorbed up to an energy, E_s, corresponding to a high harmonic. The emitted spectrum is of the Rayleigh–Jeans form below E_s, and is exponentially cut off above it (Petrosian 1981; Takahara & Tsuruta 1982). Zdziarski (1986) has derived an expression for E_s without taking into account the angular dependence of the synchrotron radiation. Here, we modify his expression to take into account the effect of angular averaging as calculated by Mahadevan, Narayan & Yi (1996) to obtain

$$\epsilon_s = \frac{343}{36} \Theta^2 \epsilon_c \ln^3 \frac{C}{\ln\left[C/\ln\left(C/\ldots\right)\right]}, \tag{9}$$

where $\epsilon_s \equiv E_s/m_e c^2$, $\epsilon_c \equiv B/B_{cr}$, the critical magnetic field strength is $B_{cr} = m_e^2 c^3/e\hbar \simeq 4.4 \times 10^{13}$ G,

$$C = \frac{3}{7\Theta}\left[\frac{\pi\tau A_M \exp(1/\Theta)}{3\alpha_f \epsilon_c}\right]^{2/7}, \tag{10}$$

α_f is the fine-structure constant and $A_M(\Theta, \epsilon_s/\epsilon_c)$ is the low-energy and low-temperature correction defined here as the ratio of equations (33) to (31) in Mahadevan et al. (1996) with coefficients given

in their table 1. The factor C above is given in the limit of $\Theta \ll 1$, appropriate for GX 339−4.

In general, any magnetic field in the source will have a strength less than that corresponding to pressure equiparition. In a hot accretion disc, the largest contribution to pressure comes from hot ions (Section 5.3), and thus $B^2/24\pi \lesssim nkT_i$. The ion temperature in the disc is found to be always subvirial, $T_i \lesssim 2 \times 10^{11}$ K (e.g. S76; Chen et al. 1997). The strongest magnetic field is achieved in an inner region, where the plasma density is largest. For estimates, we take a region with the size $R \sim 15GM_X/c^2$, where dissipation per unit logarithmic radius is maximized. In a disc-like geometry, hydrostatic equilibrium implies $H/R \simeq 1$ around $\dot{M}_{max}$ (e.g. Z98). For $\tau \sim 1$ fitted in the slab geometry (Sections 5.1 and 5.2), equipartition then corresponds to $B \simeq 2 \times 10^7$ G. Equations (9) and (10) then yield $E_s \simeq 10$ eV, or $\epsilon_s \simeq 2 \times 10^{-5}$ ($A_M \sim 0.1$ for the parameters used above).

Photons in the resulting self-absorbed spectrum undergo Compton upscattering in the thermal plasma. The spectral index of the Comptonized emission, $\Gamma \simeq 1.75$ (see Table 2), implies a certain ratio between the Comptonized luminosity and that in the seed photons (see Zdziarski 1986). Assuming a source area of $2\pi R^2$, the Comptonized synchrotron luminosity is approximately

$$L_{CS} \simeq \frac{10m_e c^3}{\lambda^3} \frac{(2\Theta)^{3-\Gamma}}{2-\Gamma} \epsilon_s^{\Gamma+1} R^2 , \qquad (11)$$

where $\lambda \simeq 2.43 \times 10^{-10}$ cm is the electron Compton wavelength. For the source parameters obtained here, $L_{CS} \simeq 3 \times 10^{34}$ erg s^{-1}. This is three orders of magnitude below the observed Xγ luminosity of $\sim 3 \times 10^{37}$ erg s^{-1}. Thus, our conclusion is that the process of thermal synchrotron emission is negligible for the formation of the Xγ spectrum provided the emitting region is similar in size to the region where the accretion energy is dissipated. Di Matteo et al. (1997) have obtained a larger L_{CS} in GX 339−4 due to their adoption of $kT \simeq 80$ keV and a much stronger B field than that derived above, and their neglection of correction to the rate of the synchrotron emission at low kT [as given in table 1 of Mahadevan et al. (1996)]. Still, $L_{CS} \sim L$ for the observations considered here would require a source size much larger than the region where gravitational energy dissipation is efficient and/or magnetic field is much above the equipartition value (equations 9–11).

We also note that the above equations imply an approximate scaling of $L_{CS}/L_E \propto M_X^{(1-\Gamma)/2}$. Thus, Comptonized thermal synchrotron emission from inner hot accretion discs around supermassive black holes in Seyfert AGNs (with typical $\Gamma \sim 1.9$, $\Theta \sim 0.2$, $\tau \sim 1$, e.g. Z97) will be even less important than in black hole binaries.

5.6　e$^\pm$ pair production

If the hot plasma is purely thermal, its parameters of $kT \sim 50$ keV and $\tau \sim 1$ imply that e$^\pm$ pair production is due to photons in the extreme Wien tail of the thermal spectrum, and thus it is very inefficient. Indeed, performing standard calculations of the pair production rate using the model spectrum as in Table 2 for the data set 1 and balancing that rate against the pair annihilation rate (e.g. Svensson 1984) leads us to the conclusion that there are almost no e$^\pm$ pairs in the plasma. Specifically, the compactness, $\ell \equiv L_{hot}\sigma_T/Rm_ec^3$, required for pair production to be able to produce pairs with the fitted τ is $\sim 10^4$ for the hot source modelled as a sphere with radius R. This corresponds to $R \sim 10^5$ cm, i.e. much less than even the Schwarzschild radius of the black hole.

We have also performed pair-balance calculations for a slab, which better approximates the disc geometry. Here, we used the

model of a slab with cold clouds in the mid-plane, see Fig. 5(d) and Section 5.1. The relevant compactness is then the local one corresponding to the power dissipated within a cube with size equal to the half-thickness, H, of the slab. The results are shown in Fig. 6, where we see that $\ell \sim 10^3 - 3 \times 10^3$ (depending on the covering factor of cold clouds, f_c). Approximating the source as a uniformly radiating disc with the outer radius R, we obtain $R^2/H = L_{hot}\sigma_T/2\pi\ell m_ec^3$, which for $H/R \sim 1$, characteristic for hot discs, yields $R \sim 10^5$ cm, which is the same value as obtained above for the spherical geometry, and much less than our estimates of the size of the hot plasma.

Thus, there are no e$^\pm$ in the hot plasma in GX 339−4 provided the plasma is fully thermal. On the other hand, it is also possible that non-thermal acceleration of selected electrons to relativistic energies operates in the source in addition to heating of the plasma. This hybrid model has been applied to NGC 4151 by Zdziarski et al. (1996) and Johnson et al. (1997) and to Cyg X-1 by Poutanen & Coppi (1998) and Poutanen (1998). We have applied that model to the data set 1. The pair-dominated hybrid model yields the same χ^2 as the thermal model (fit 1c in Table 2) for any $\ell \gtrsim 150$, and the 90 per cent confidence lower limit is $\ell_{min} \simeq 70$ (for spherical geometry). The fraction of the power that is supplied to the accelerated electrons and pairs is $\simeq 0.09$ at ℓ_{min}, and it decreases with increasing ℓ. This ℓ_{min} implies $R < 10^7$ cm, which corresponds to $r \lesssim 20$ for $M_X = 3$ M$_\odot$. This is in principle compatible with the expected size of a hot accretion disc ($r \gg 6$).

We have also applied the hybrid model to the data obtained from the entire OSSE observation of the source, 1991 September 5–12 (G95), which have much better statistical quality than either of our OSSE data sets. We find that these data are fitted somewhat better, $\Delta\chi^2 = -4$, by the hybrid model than by the pure thermal one (which gives $kT = 62^{+13}_{-9}$ keV at fixed $\Omega/2\pi = 0.44$). The residuals in the thermal model show a weak high-energy tail on top of the thermal spectrum above ~ 300 keV. This may hint at the presence of non-thermal pairs, accounting for the tail. In the hybrid model, $\ell = 150^{+\infty}_{-30}$, and the non-thermal fraction at the best fit is $\simeq 0.05$. On the other hand, G95 show softening of the spectrum of GX 339−4 with time during that observation. Therefore, the tail could also be an artefact of fitting the spectrum averaged over a range of plasma parameters by a single-component thermal model.

6　COMPARISON WITH BLACK HOLE AND NEUTRON STAR SOURCES

In this section, we compare our Xγ spectrum of GX 339−4 with those of established black hole and neutron star sources. Our objective is to determine whether the Xγ spectrum of GX 339−4 is indeed similar to those seen in black hole sources but not to those seen in accreting neutron stars. We stress that both black hole binaries and neutron star binaries exhibit two main spectral states, X-ray low (hard) and high (soft), and only the corresponding states should be directly compared.

6.1　Xγ emission of black hole sources

6.1.1　Black-hole binaries in the hard state

Hard-state X-ray spectra of the archetypical black hole binary Cyg X-1 have been fitted by G97. Their fit to the average *Ginga* data of 1991 June 6 with a power law and reflection model (as in Section 4) yields $\Gamma = 1.59^{+0.03}_{-0.03}$ and $\Omega/2\pi = 0.34^{+0.05}_{-0.05}$, which is rather similar to our spectra of GX 339−4. X-ray spectra with similar power law

indices and moderately weak Compton reflection components are seen from other black hole binaries in the hard (low) state, e.g. Nova Muscae (Ebisawa et al. 1994; Życki et al. 1998) and GS 2023+338 (Życki et al. 1997).

The broad-band Xγ spectra of Cyg X-1 in G97 are also similar to that of GX 339−4, and well modelled by a primary continuum resulting from thermal Comptonization in a plasma with similar τ, but higher electron temperature, $kT \sim 100$ keV (and with an additional small spectral component from emission of a plasma with $\tau \gg 1$). Soft γ-ray spectra similar in shape to that of Cyg X-1 have been observed from other black hole binaries in the hard state (e.g. Grove et al. 1998; Grebenev, Sunyaev & Pavlinsky 1997).

Motivated by the similarity, we test here the hot accretion disc model of Z98 (see Section 5.3) against the Cyg X-1 data. We have refitted the spectrum of G97 corresponding to the peak flux using the hot slab model used in Section 5.1 for the primary continuum, and obtained $y \simeq 0.4$ and $\tau \simeq 0.5$ (assuming $f_c = 0.1$). Those parameters imply $\alpha \simeq 0.4$ using $\tau(\dot{M}_{max})$ of equation (6). The peak luminosity in the hard state is about 4×10^{37} erg s^{-1}, for which equation (7) implies $M_X \gtrsim 10$ M$_\odot$. This agrees well with the best estimates of the mass of Cyg X-1 (e.g. van Paradijs & McClintock 1995). Thus, it is possible that a hot accretion disc is present in the hard state of black hole binaries, and that its structure determines both the observed optical depth of the hot plasma and the maximum luminosity in the hard state.

6.1.2 Seyfert 1s

It is of great interest that the Xγ spectra of black hole binaries in the hard state are similar to the spectra of Seyfert 1 AGNs; this similarity in the X-ray regime was pointed out by Tanaka (1989). Specifically, both classes of objects show power-law X-ray spectra with $\Gamma \sim 1.7$–2, Compton reflection components with Fe Kα lines, and high-energy cut-offs above ~ 100 keV (e.g. Z97). The cut-offs can be modelled in both cases by Comptonization with $\tau \sim 1$ and $kT \sim 100$ keV (Z97).

Here, we point out that the intrinsic spectrum above 4 keV of GX 339−4 appears virtually identical to that of NGC 4151, which, in soft γ-rays, is the brightest and best-studied Seyfert AGN. We note

here that apart from strong absorption, the Xγ spectrum of NGC 4151 appears rather typical for Seyfert 1s, and the OSSE spectra of NGC 4151 and of all other Seyfert 1s observed by OSSE are very similar (Zdziarski et al. 1996; Z97). Also, the intrinsic Xγ spectrum of NGC 4151 is very similar to that of a 'typical' Seyfert 1, NGC 5548 (Magdziarz et al. 1998). This makes models specially designed for NGC 4151 (e.g. Poutanen et al. 1996) probably unnecessary. The thermal Comptonization fit (after applying the same correction to solutions of the Kompaneets equation as in Section 4 above) to a joint *ROSAT/Ginga*/OSSE spectrum of NGC 4151 (Zdziarski et al. 1996) yields $\Gamma = 1.81^{+0.04}_{-0.04}$, $kT = 63^{+19}_{-11}$ keV, and $\Omega/2\pi = 0.49^{+0.26}_{-0.26}$, which are consistent within errors with those given in Table 2 for GX 339−4. We find that the form of the high-energy cut-off is almost the same in both sources, as shown in Fig. 9, which shows the ratio of the OSSE spectrum of GX 339−4 (from the entire observation of 1991 September 5–12) to the spectrum of NGC 4151 averaged over all OSSE observations (from Johnson et al. 1997).

6.2 Xγ emission of weakly magnetized accreting neutron-stars

Two types of objects, the Xγ emission of which (if present) is unambiguously connected with neutron stars, are X-ray pulsars and isolated neutron stars. Those Xγ sources possess strong magnetic fields, $B \gtrsim 10^{11}$ G, and their emission can be easily distinguished from that of black hole systems, see Finger & Prince (1997) and Thompson et al. (1997) for recent reviews.

On the other hand, weakly magnetized accreting neutron stars often show X-ray emission very similar to that of black hole binaries. Some LMXBs classified as black hole candidates have been subsequently found to emit type 1 X-ray bursts, leading to their identification as neutron-star binaries. A recent example is the discovery of X-ray bursts from GS 1826−238 (Bazzano et al. 1997), a source that appeared as a black hole candidate in Tanaka (1989).

Indeed, X-ray emission of X-ray bursters in their hard (low) state can be very similar to that of GX 339−4. For example, two *Ginga* observations of 4U 1608−522 show a power-law component with $\Gamma \simeq 1.9$ accompanied by Compton reflection from a strongly ionized medium with $\Omega/2\pi \sim 0.5$ in the ~ 2–60 keV range (Yoshida et al. 1993). Similarly, GS 1826−238 observed by *Ginga* has $\Gamma \sim 1.8$ and Compton reflection (Strickman et al. 1996). Thus, X-ray spectra alone appear to be insufficient to distinguish a weakly magnetized neutron star from a black hole.

On the other hand, typical spectra of X-ray bursters observed in the ~ 30–200 keV range by the SIGMA telescope on board *GRANAT* and the BATSE detector on board *CGRO* are rather soft; see the reviews by Barret & Vedrenne (1994), van der Klis (1994), Vargas et al. (1997) and Tavani & Barret (1997). In most cases, the spectra can be fitted equally well by a power law with $\langle \Gamma \rangle \sim 3$ or thermal Comptonization with $\langle kT \rangle \sim 15$–20 keV. There is only one reported OSSE detection of an X-ray burster, GS 1826−238, which shows a similar $\Gamma = 3.1 \pm 0.5$ above 50 keV (Strickman et al. 1996). These spectra are all much softer than the corresponding spectra of black hole binaries in the hard state [but note their similarity to black hole binary spectra in the soft state (Grove et al. 1998)].

Unfortunately, there have been almost no observations below 30 keV simultaneous with those at $\gtrsim 30$ keV discussed above. Therefore, there is no information on the X-ray spectral state (high or low) of the bursters during most of those observations. However, X-ray bursters are rather often found in the low state when observed in X-rays alone, and thus we can assume that some of the spectra
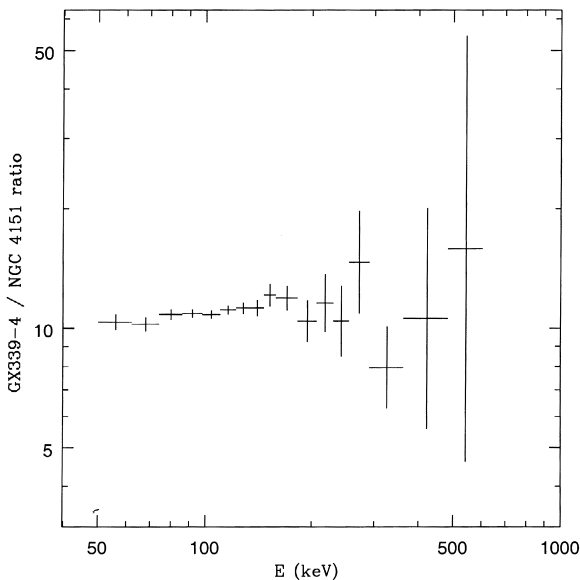

Figure 9. The ratio of the OSSE spectrum of GX 339–4 from 1991 September 5–12 to the average OSSE spectrum of the Seyfert NGC 4151.

observed at $\gtrsim 30$ keV correspond to the X-ray low, hard, state. This then implies that the Xγ spectra of bursters in the low state have spectral breaks at energies significantly below 100 keV, or have thermal Comptonization temperatures of $kT \lesssim 30$ keV. This conclusion is indeed confirmed by a ~ 2–250 keV observation of 4U 1608–522 in the low state simultaneously by *Ginga* and BATSE, which yields a break at ~ 60 keV in the broken power-law model or $kT \sim 25$ keV, $\tau \gg 1$, in the thermal Comptonization model (Zhang et al. 1996). A similar spectral break at ~ 60 keV was also seen in a 30–200 keV observation of 4U 1728–34 (Claret et al. 1994).

6.3 Spectral black hole-signatures

As discussed above, X-ray bursters in the low state have Xγ emission with breaks or cut-offs at significantly *lower* energies than both that seen in GX 339–4 and those found in black hole binaries in the hard (low) state in general (Section 6.1.1). When the spectra are fitted by the thermal Comptonization model (with $\tau \gtrsim 1$), $kT \lesssim 30$ keV and $kT \gtrsim 50$ keV for neutron stars and black holes, respectively. We propose this quantitative criterion to be a black hole signature.

We see that these two ranges of temperature are not far apart, and it is important to test this criterion against available data. Those tests should take into account Compton reflection and relativistic effects in thermal Comptonization, and use broad-band Xγ data. These criteria are not satisfied by thermal Comptonization fits in Mandrou et al. (1994) and Churazov et al. (1994), who find $kT = 33$ keV and 38 keV, respectively, in GRS 1758–258, a black hole candidate in the hard state (Sunyaev et al. 1991). Those fits use the non-relativistic model of Sunyaev & Titarchuk (1980), neglect reflection, and are in a 35–250 keV range only. In fact, very similar assumptions lead to a gross underestimate of the temperature in Cyg X-1 in the hard state, $kT = 27$ keV (Sunyaev & Trümper 1979), whereas $kT \sim 100$ keV is obtained from broad-band spectra fitted by a relativistic Comptonization model with reflection (e.g. G97).

As a caveat, we mention that a 40–200 keV SIGMA spectrum of a source in the Terzan 2 globular cluster appears to have no cut-off up to 200 keV and $\Gamma \simeq 1.7 \pm 0.5$ (Barret & Vedrenne 1994; Barret et al. 1991). Such a spectrum may imply a Comptonization temperature $\gtrsim 100$ keV, which is characteristic of black hole sources but not of neutron-star ones, whereas the same cluster contains an X-ray burster, X1724–308. Our proposed black-hole signature would not hold if the emission observed by SIGMA indeed had $\gamma \sim 1.7$ extending to 200 keV (which is not certain, taking into account the large statistical errors) and if it originated from the burster (for which there is also no certainty). On the other hand, a recent observation of Terzan 2 by *RXTE*, which is an instrument much more sensitive than SIGMA, shows a spectrum well fitted by thermal Comptonization with $kT \simeq 30$ keV, in agreement with our criterion above (Barret et al., in preparation).

Finally, we point out that the presence of power-law emission with $\Gamma \sim 2.5$–3 in the ~ 30–500 keV range, which is seen from black hole binaries in the soft state (Grove et al. 1998), may not constitute a black hole signature, in spite of a recent claim (Titarchuk 1997). Very similar soft single power-law spectra without detectable high-energy breaks are seen from many X-ray bursters (e.g. Barret et al. 1992; Goldwurm et al. 1996; Harmon et al. 1996).

7 CONCLUSIONS

The results of this work can be divided into two main parts as far as dependence on model assumptions is concerned. The results of Sections 2, 3, 4 and 6 are relatively model-independent.

In Section 2, we determine the distance to the object to be > 3 kpc, with 4 kpc being the most likely value. We show that the most recent distance determination of ~ 1.3 kpc is in error. We also find $E(B - V) \simeq 1.2$ and $N_H \simeq 6 \times 10^{21}$ cm^{-2} as mutually consistent most likely values. The mass of the compact object appears relatively low, $M_X \lesssim 5$ M$_\odot$.

In Sections 3 and 4, we present our data and show that the spectra can be very well fitted by Comptonization in a thermal plasma with $kT \simeq 50$ keV and $\tau \sim 1$. In addition, we find, at very high significance, the presence of Compton reflection from an ionized medium and a soft X-ray excess.

In Section 6, we show that this spectrum is similar to that of other black hole binaries, as well as to those of Seyfert AGNs. After comparison with spectra of neutron star sources, we propose that a thermal Comptonization temperature of $kT \gtrsim 50$ keV represents a black hole signature.

Physical interpretation of our results is given in Section 5. Here, we study the constraints following from the Xγ spectra and concentrate on accretion disc and corona models. We do not consider models with large-scale outflows or jets. As the Xγ observations were not accompanied by observations in any other wavelength, we do not discuss such data (e.g. optical, Motch et al. 1983) obtained at other epochs. We also do not discuss time variability of the source.

With these caveats, our best physical model is that of a hot accretion disc within ~ 100 gravitational radii surrounded by a cold outer disc; see Figs 5(d) and (e). The seed photons for thermal Comptonization in the hot disc are supplied by cold clouds within the hot disc. The emission of the hot disc is Compton-reflected by the outer cold disc. The outer disc also emits most of the observed soft X-ray excess. This model is in agreement with the spectra, energy balance, and ionization balance at the surface of the reflecting outer disc. The observed amount of reflection requires that the outer disc is flared.

The hot disc accretion rate is near the maximum set by advection. Based on the spectral fit of the hot slab model, we find a viscosity parameter of $\alpha \sim 1$ and $M_X \gtrsim 3$ M$_\odot$, a mass that is in agreement with the dynamical mass determination. The hot disc model, for which parameters are independent of M_X, is also supported by the observed similarity of the spectrum of GX 339–4 to those of Seyfert 1s.

We find that e$^\pm$ pair production photons in the thermal Comptonization spectrum is negligible and thus the disc is most likely made of electrons and ions (although more complex models with e$^\pm$ pairs are possible). Also, synchrotron emission in the hot disc with equipartition magnetic field is negligible as a source of seed photons for Comptonization.

We can rule out models with a cold disc covered by a homogeneous corona or by active regions located on the surface of the disc as violating the energy balance. On the other hand, the energy balance is satisfied if there are active regions at some height above the disc surface. However, this model provides poor fits to the spectral data; the predicted ionization state of the postulated inner cold disc is much higher than that found from the Compton reflection spectral component, as well as predicting an Ω–Γ correlation opposite to that observed.

REFERENCES

Abramowicz M. A., Czerny B., Lasota J.-P., Szuszkiewicz E., 1988, ApJ, 332, 646

Abramowicz M. A., Chen X., Kato S., Lasota J.-P., Regev O., 1995, ApJ, 438, L37

Alcaino G., 1971, A&A, 11, 7

Anders E., Ebihara M., 1982, Geochim. Cosmochim. Acta, 46, 2363

Arnaud K. A., 1996, in Jacoby G. H., Barnes J., eds, ASP Conf. Ser. Vol. 101, Astronomical Data Analysis Software and Systems V. Astron. Soc. Pac., San Francisco, p. 17

Barret D., Vedrenne G., 1994, ApJS, 92, 505

Barret D. et al., 1991, ApJ, 379, L21

Barret D. et al., 1992, ApJ, 394, 615

Bazzano A., Cocchi M., Natalucci L., Ubertini P., Heise J., in't Zand J., Muller J. M., Smith M. J. S., 1997, in Dermer C. D., Strickman M. S., Kurfess J. D., eds, The 4th Compton Symposium. AIP, New York p. 729

Burton W. B., 1992, in Burton W. B., Elmgreen B. G, Genzel R., eds, The Galactic Interstellar Medium. Springer, Berlin, p. 53

Callanan P. J., Charles P. A., Honey W. B., Thorstensen J. R., 1992, MNRAS, 259, 395 (C92)

Celotti A., Fabian A. C., Rees M. J., 1992, MNRAS, 255, 419

Chen X., Abramowicz M. A., Lasota J. P., 1997, ApJ, 476, 61

Churazov E. et al., 1994, ApJS, 92, 381

Claret A. et al., 1994, ApJ, 423, 436

Collin-Souffrin S., Czerny B., Dumont A.-M., Życki P. T., 1996, A&A, 314, 393

Coppi P. S., 1992, MNRAS, 258, 657

Corbet R. H. D., Thorstensen J. R., Charles P. A., Honey W. B., Smale A. P., Menzies J. W., 1987, MNRAS, 227, 1055

Cowley A. P., Crampton D., Hutchings J. B., 1987, AJ, 92, 195 (C87)

Di Matteo T., Celotti A., Fabian A. C., 1997, MNRAS, 291, 705

Diplas A., Savage B. D., 1994, ApJ, 427, 274

Done C., Mulchaey J. S., Mushotzky R. F., Arnaud K. A., 1992, ApJ, 395, 275

Ebisawa K. et al., 1994, PASJ, 46, 375

Ebisawa K., Ueda Y., Inoue H., Tanaka Y., White N. E., 1996, ApJ, 467, 419

Fabian A. C., Guilbert P. W., Motch C., Ricketts M., Ilovaisky S. A., Chevalier C., 1982, A&A, 111, L9

Fabian A. C., Rees M. J., Stella L., White N. E., 1989, MNRAS, 238, 729

Finger M. H., Prince T. A., 1997, in Dermer C. D., Strickman M. S., Kurfess J. D., eds, The 4th Compton Symposium. AIP, New York, p. 57

FitzGerald M. P., 1987, MNRAS, 229, 227

FitzGerald M. P., Jackson P. D., Moffat A. F. J., 1977, Observatory, 97, 129

Galeev A. A., Rosner R., Vaiana G. S., 1979, ApJ, 229, 318

George I. M., Fabian A. C., 1991, MNRAS, 249, 352

Gierliński M., Zdziarski A. A., Done C., Johnson W. N., Ebisawa K., Ueda Y., Haardt F., Phlips B. F., 1997, MNRAS, 288, 958 (G97)

Goldwurm A. et al., 1996, A&A, 310, 857

Grabelsky D. A. et al., 1995, ApJ, 441, 800 (G95)

Grebenev S. A., Sunyaev R. A., Pavlinsky M. N., 1997, Adv. Space Res., 19, (1) 15

Grindlay J. E., 1979, ApJ, 232, L33

Grove J. E., Johnson W. N., Kroeger R. A., McNaron-Brown K., Skibo J. G., 1998, ApJ, 500, 899

Haardt F., Maraschi L., 1993, ApJ, 413, 507

Haardt F., Maraschi L., Ghisellini G., 1994, ApJ, 432, L95

Haensel P., 1995, in Roxburgh I. A., Masnou J.-L., eds, Lecture Notes in Physics 458, Physical Processes in Astrophysics. Springer, Berlin, p. 49

Harmon B. A. et al., 1994, ApJ, 425, L17

Harmon B. A., Wilson C. A., Tavani M., Zhang S. N., Rubin B. C., Paciesas W. S., Ford E. C., Kaaret P., 1996, A&AS, 120 (III), 197

Ichimaru S., 1977, ApJ, 214, 840

Ilovaisky S. A., Chevalier C., 1981, IAU Circ. 3856

Ilovaisky S. A., Chevalier C., Motch C., Chiapetti L., 1986, A&A, 164, 67

Johnson W. N. et al., 1993, ApJS, 86, 693

Johnson W. N., McNaron-Brown K., Kurfess J. D., Zdziarski A. A., Magdziarz P., Gehrels N., 1997, ApJ, 482, 173

Kaastra J. S., Mewe R., 1993, A&AS, 97, 443

Krolik J. H., 1998, ApJ, 498, L13

Kuncic Z., Celotti A., Rees M. J., 1997, MNRAS, 284, 717

Lightman A. P., Eardley D. M., 1974, ApJ, 187, L1

Lightman A. P., White T. R., 1988, ApJ, 335, 57

Lindoff U., 1972, A&AS, 7, 231

Magdziarz P., Zdziarski A. A., 1995, MNRAS, 273, 837

Magdziarz P., Blaes O. M., Zdziarski A. A., Johnson W. N., Smith D. A., 1998, MNRAS, 301, 179

Mahadevan R., Narayan R., Yi I., 1996, ApJ, 465, 327

Makino F., the ASTRO-C team, 1987, Astrophys. Lett. Commun., 25, 223

Makishima K. et al., 1986, ApJ, 308, 635

Mandrou P. et al., 1994, ApJS, 92, 343

Matt G., Fabian A. C., Ross R. R., 1993, MNRAS, 262, 179

Mauche C. W., Gorenstein P., 1986, ApJ, 302, 371

Mermilliod J.-C., Mermilliod M., 1994, Catalogue of Mean UBV Data on Stars. Springer, Berlin

Milson J. A., Chen X., Taam R. E., 1994, ApJ, 421, 668

Miyamoto S., Kimura K., Kitamoto S., Dotani T., Ebisawa K., 1991, ApJ, 383, 784

Moffat A. F. J., Vogt N., 1973, A&AS, 10, 135

Moffat A. F. J., Vogt N., 1975, A&AS, 20, 155

Motch C., Ricketts M. J., Page C. G., Ilovaisky S. A., Chevalier C., 1983, A&A, 119, 171

Nandra K., Pounds K. A., 1994, MNRAS, 268, 405

Narayan R., 1996, ApJ, 462, 136

Narayan R., Yi I., 1995, ApJ, 452, 710

Neckel T., Klare G., 1980, A&AS, 42, 251

Petrosian V., 1981, ApJ, 251, 727

Podsiadlowski P., 1991, Nat, 350, 136

Poutanen J., 1998, in Abramowicz M. A., Björnsson G., Pringle J. E., eds, Theory of Black Hole Accretion Discs. Cambridge Univ. Press, Cambridge, in press (astro-ph/9805025)

Poutanen J., Coppi P. S., 1998, Phys. Scr., in press (astro-ph/9711316)

Poutanen J., Svensson R., 1996, ApJ, 470, 249

Poutanen J., Sikora M., Begelman M. C., Magdziarz P., 1996, ApJ, 465, L107

Poutanen J., Krolik J. H., Ryde F., 1997, MNRAS, 292, L21

Predehl P., Bräuninger H., Burkert W., Schmitt J. H. M. M., 1991, A&A, 246, L40

Press W. H., Teukolsky S. A., Vetterling W. T., Flannery B. P., 1992, Numerical Recipes. Cambridge Univ. Press, Cambridge

Pringle J. E., 1976, MNRAS, 177, 65

Reilman R. F., Manson S. T., 1979, ApJS, 40, 815

Rubin B. C., Harmon B. A., Paciesas W. S., Robinson C. R., Zhang S. N., Fishman G. J., 1998, ApJ, 492, L67

Rybicki G. R., Lightman A. P., 1979, Radiative Processes in Astrophysics. Wiley-Interscience, New York

Shakura N. I., Sunyaev R. A., 1973, A&A, 24, 337

Shakura N. I., Sunyaev R. A., 1976, MNRAS, 175, 613

Shapiro S. L., Lightman A. P., Eardley D. M., 1976, ApJ, 204, 187 (S76)

Scheffler H., Elsasser H., 1987, Physics of the Galaxy and Interstellar Matter. Springer, Berlin

Shimura T., Takahara F., 1995, ApJ, 445, 780

Smale A. P., 1996, in Evans A., Wood J. H., eds, Cataclysmic Variables and Related Objects. Kluwer, Amsterdam, p. 347

Stern B. E., Poutanen J., Svensson R., Sikora M., Begelman M. C., 1995, ApJ, 449, L13

Strickman M., Skibo J., Purcell W., Barret D., Motch C., 1996, A&AS, 120 (III), 217

Sunyaev R. A., Titarchuk L. G., 1980, A&A, 86, 121

Sunyaev R. A., Trümper J., 1979, Nat, 279, 506

Sunyaev R. A. et al., 1991, A&A, 247, L29

Svensson R., 1984, MNRAS, 209, 175

Svensson R., Zdziarski A. A., 1994, ApJ, 436, 599

Takahara F., Tsuruta S., 1982, Prog. Theor. Phys., 67, 485

Tanaka Y., 1989, in Hunt J., Battrick B., eds, 23rd ESLAB Symposium, ESA SP-296. ESA, Noordwijk, p. 3

Tanaka Y., Lewin W. H. G., 1995, in Lewin W. H. G., van Paradijs J., van den Heuvel E. P. J., eds, X-Ray Binaries. Cambridge Univ. Press, Cambridge, p. 126

Tavani M., Barret D., 1997, in Dermer C. D., Strickman M. S., Kurfess J. D., eds, The 4th Compton Symposium. AIP, New York, p. 75

Tavani M., London R., 1993, ApJ, 410, 281

Titarchuk L., 1997, in Winkler C., Courvoisier T., Durouchoux P., eds, The Transparent Universe, ESA SP-382. ESA, Noordwijk, p. 163

Thompson D. J, Harding A. K., Hermsen W., Ulmer M. P., 1997, in Dermer C. D., Strickman M. S., Kurfess J. D., eds, The 4th Compton Symposium. AIP, New York, p. 39

Turner M. J. L. et al., 1989, PASJ, 41, 345

Ueda Y., Ebisawa K., Done C., 1994, PASJ, 46, 107 (U94)

van der Klis M., 1994, ApJS, 92, 511

van Paradijs J., McClintock J. E., 1995, in Lewin W. H. G., van Paradijs J., van den Heuvel E. P. J., eds, X-Ray Binaries. Cambridge Univ. Press, Cambridge, p. 58

Vargas M. et al., 1997, in Winkler C., Courvoisier T., Durouchoux P., eds, The Transparent Universe, ESA SP-382. ESA, Noordwijk, p. 129

Vázquez R. A., Feinstein A., 1992, A&AS, 92, 863

Vrtilek S. D., Raymond J. C., Garcia M. R., Verbunt F., Hasinger G., Kürster M., 1990, A&A, 235, 162

Vrtilek S. D., McClintock J. E., Seward F. D., Kahn S. M., Wargelin B. J., 1991, ApJS, 76, 1127

Webbink R. F., Rappaport S., Savonije G. J., 1983, ApJ, 270, 678

Wu X.-B., 1997, MNRAS, 292, 113

Yoshida K., Mitsuda K., Ebisawa K., Ueda Y., Fujimoto R., Yaqoob T., Done C., 1993, PASJ, 45, 605

Zdziarski A. A., 1985, ApJ, 289, 514

Zdziarski A. A., 1986, ApJ, 303, 94

Zdziarski A. A., 1998, MNRAS, 296, L51 (Z98)

Zdziarski A. A., Johnson W. N., Magdziarz P., 1996, MNRAS, 283, 193

Zdziarski A. A., Johnson W. N., Poutanen J., Magdziarz P., Gierliński M., 1997, in Winkler C., Courvoisier T., Durouchoux P., eds, The Transparent Universe, ESA SP-382. ESA, Noordwijk, p. 373 (Z97)

Zhang S. N. et al., 1996, A&AS, 120 (III), 279

Życki P. T., Czerny B., 1994, MNRAS, 266, 653

Życki P. T., Done C., Smith D. A., 1997, ApJ, 488, L113

Życki P. T., Done C., Smith D. A., 1998, ApJ, 496, L25

This paper has been typeset from a T$_E$X/L^{A}T$_E$X file prepared by the author.